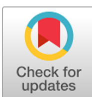

Advances in Optics and Photonics

Recent advances in light sources on silicon

Yu Han,[1,5] **Hyundai Park,**[2] **John Bowers,**[3] **and Kei May Lau**[4,6]

[1] State Key Laboratory of Optoelectronic Materials and Technologies, School of Electronics and Information Technology, Sun Yat-sen University, Guangzhou 510275, China
[2] Nexus Photonics, 6500 Hollister Avenue, Ste. 140 Goleta, California 93117, USA
[3] Department of Electrical and Computer Engineering, University of California Santa Barbara, Santa Barbara, California 93106, USA
[4] Department of Electronic and Computer Engineering, Hong Kong University of Science & Technology, Clear Water Bay, Hong Kong, China
[5] e-mail: hany87@mail.sysu.edu.cn
[6] e-mail: eekmlau@ust.hk

Received February 11, 2022; revised April 29, 2022; accepted May 3, 2022; published 5 August 2022

Realizing efficient on-chip light sources has long been the “holy-grail” for Si-photonics research. Several important breakthroughs were made in this field in the past few years. In this article, we review the most recent advances in light sources integrated onto mainstream Si platforms and discuss four different integration technologies: Group IV light sources on Si, heterogeneous integration of III–V light sources on Si, blanket heteroepitaxy of III–V light sources on Si, and selective heteroepitaxy of III–V light sources on Si. We start with briefly introducing the basic concepts of each technology and then focus on the recent progress via presenting the most representative device demonstrations. Finally, we discuss the research challenges and opportunities associated with each technology. © 2022 Optica Publishing Group

https://doi.org/10.1364/AOP.455976

1. Introduction . . . 406
2. Group IV Light Sources . . . 407
   2.1. Si-Based Light Sources . . . 408
   2.2. Ge-Based Light Sources . . . 409
   2.3. GeSn-Based Light Sources . . . 410
      2.3a. Optically Pumped GeSn Lasers . . . 411
      2.3b. Electrically Pumped GeSn Lasers . . . 412
3. Heterogeneous Integration of III-V Light Sources on Si . . . 413
   3.1. Die/Wafer Bonding . . . 414
      3.1a. Concept of Bonding . . . 414
      3.1b. High-Performance III–V/Si Light Sources . . . 416
   3.2. Micro-Transfer Printing . . . 417
      3.2a. Concept of Micro-Transfer Printing . . . 417
      3.2b. III–V-on-Si Light Sources . . . 419

4. Blanket Heteroepitaxy of III-V Light Sources on Si 420
4.1. GaAs-Based Light Sources 421
4.1a. GaAs Thin Films Grown on Si 421
4.1b. 1.3 μm QD Lasers on GaAs/Si Templates 421
4.2. InP-Based Light Sources 423
4.2a. InP Thin Films Grown on Si 423
4.2b. 1.55 μm Lasers on InP/Si Templates 424
4.3. GaSb-Based Light Sources 425
4.3a. GaSb Thin Films Grown on Si 425
4.3b. Mid-Infrared Lasers on GaSb/Si Templates 426
5. Selective Heteroepitaxy of III-V Light Sources on Si 428
5.1. Vertical Integration Schemes 429
5.1a. Aspect Ratio Trapping 429
5.1b. Nano-Ridge Engineering 431
5.2. Lateral Integration Schemes 433
5.2a. Template-Assisted Selective Epitaxy 433
5.2b. Lateral ART 434
6. Summary and Perspective 436
Disclosures 438
Data availability 438
References 438

Recent advances in light sources on silicon

Yu Han, Hyundai Park, John Bowers, and Kei May Lau

1. INTRODUCTION

Si-photonics is emerging as a highly competitive technology to address the "communication bottleneck" in present data centers and high-performance computing systems where issues associated with the power and speed of conventional electrical interconnects have become increasingly pressing [1,2,3]. Replacing electrons with photons to transmit data brings advantages including high-speed operation, low power consumption, and high-capacity transmission. Building photonic integrated circuits (PICs) on industry-standard Si platform promises additional merits, namely ultra-low cost, mass manufacturing, large integration density, and high scalability. These features are essential for future consumer-oriented applications such as automobile, metrology, and bio/chemical sensing [4]. In addition, constructing PICs on Si simplifies co-integration with Si-microelectronics and the realization of high-performance and multi-functional Si-based optoelectronic integrated circuits (OEICs) [5].

Benefiting from an excellent Si/SiO_2 interface and a large index contrast, Si is an ideal platform for implementing passive optical devices. Examples include low-loss waveguides, mode converters, and multiplexers/demultiplexers [6]. Although Si is a centrosymmetric crystal and, thus, not an ideal material for optical modulators, high-performance modulators using the plasma dispersion effect have been demonstrated and commercialized [7]. Ge-based photodetectors (PDs) operating in the telecom band can also be selectively grown on Si-photonics wafers using chemical vapor deposition, and this standardized process is now available in multiple foundries [8]. Furthermore, together with SiN and Ge waveguides, Si-based PICs can operate over a wide range of wavelengths, ranging from the visible band all the way to the mid-infrared region. Accordingly, Si photonics is an enabling platform for a variety of applications encompassing display, computing, communication, sensing, etc. [9–15].

Although Si can efficiently transmit, modulate, and detect light, the indirect band structure of Group IV semiconductors precludes efficient light emission. An on-chip light emitter therefore has long remained the last missing building block for Si-based PICs [16]. Early commercially available Si-based PICs often employed an off-chip III–V light source using either edging coupling or flip-chip integration [17,18]. However, these approaches limit the further scaling of Si-photonics. Targeting at benefits in terms of size, cost and power consumption, a variety of technologies have been developed to obtain efficient on-chip lasers on Si in the past 20 years [19–22]. Research in the early 2000s focused on engineering Si for enhanced light emission, and later moved to Ge in early 2010s and recently to GeSn alloys because a direct bandgap is vital for efficient room-temperature laser operation [23,24]. Meanwhile, efforts in integrating mature III–V light sources on Si started in the mid-2000s. Heterogeneous integration approaches including die/wafer bonding and micro-transfer printing were developed and later commercialized [25,26]. Monolithically integrating III–V light sources on Si using direct heteroepitaxy was revived in the 2010s [27]. This resurrected interest was driven by two factors. First, quantum dots (QDs) were shown to be more tolerant to crystalline defects and, thus, promised improved device reliability for lasers grown on Si [28]. Second, novel growth schemes were designed to produce low

Table 1. Comparison of Different Technologies of Integrating Light Sources on Si

Approaches		Ge/Sn Lasers on Si	Heterogeneous Integration of III–V Lasers on Si	Blanket Heteroepitaxy of III–V Lasers on Si	Selective Heteroepitaxy of III–V Lasers on Si
Technology pros and cons	Integration density	High	Medium	High	High
	CMOS compatibility	Compatible	Back-end compatible	Potentially front-end compatible	Potentially front-end compatible
	Throughput	High	Medium	High	High
	Cost	Low	Medium	Low	Low
	Maturity	Early R&D	Commercialized	R&D	R&D
Metrics of light sources on Si	Crystalline quality	High TD density	Excellent	Low TD density for GaAs, high TD for InP and GaSb on Si	Low TD density
	Wavelength	Mid-infrared	Not limited	Not limited	Not limited
	Electrically driven devices	Yes	Yes	Yes	Not yet
	RT operation	Not yet	Yes	Yes	Yes
	Light coupling with Si-WG	Challenging for epitaxial lasers	Yes	Challenging	Yes
	Thermal impedance	Low	Medium	Low	Low

threading dislocation (TD) density or even TD-free III–V semiconductors on Si [29]. Table 1 compares the pros and cons of each integration technology and summarizes the metrics of light sources on Si using different approaches. Each integration approach often overcomes some of the issues of the others while still has its own unique challenges.

In this article, we review the most recent advances in light sources on Si using four different integration technologies. This paper is organized as follows: Section 2 examines building on-chip light emitters using Group IV semiconductors with an emphasis on GeSn-based light sources. Section 3 focuses on heterogeneous integration of III–V lasers on Si using die/wafer bonding and micro-transfer printing, and presents several representative high-performance laser sources that synergize the merits of both Group IV and Group III–V semiconductors. Section 4 discusses the monolithic integration of III–V light sources on Si via direct heteroepitaxy and centers on the latest progresses of III–V/Si complaint substrates with low TD density and laser diodes grown on Si with high reliability. Section 5 concentrates on the selective area growth of III–V light sources on Si and highlights its potential for close integration and efficient light coupling with Si-based optical components. Finally, Section 6 provides a brief perspective for light sources on Si as well as a summary of this review.

2. GROUP IV LIGHT SOURCES

The pursuit of Group IV light sources is mainly driven by the material and process compatibility with the existing complementary metal–oxide–semiconductor (CMOS) foundry [6]. Group IV lasers grown on Si, if successfully demonstrated, represent a monolithic integration solution for fully integrated Si-based PICs, which could potentially enable a similar throughput and scalability as Si-based microelectronics.

Constructing efficient light sources usually requires semiconductors with a direct bandgap, and the market is traditionally and currently dominated by Group III–V compound semiconductors such as GaAs and InP [30]. Group IV materials, namely Si and Ge, however, feature an inherent indirect band structure. In their bulk states, light emission is a phonon-assisted process with an extremely low probability, and other non-radiative processes including Auger recombination and free carrier absorption further compromise the light-emitting efficiency of Group IV semiconductors [31].

Early efforts in building Si-based light sources focused on improving the radiative recombination as well as reducing the non-radiative processes via a variety of techniques [32]. As the light-emitting efficiency is still unsatisfactory, other approaches were subsequently investigated including introducing foreign light emitting centers, for example Erbium, and exploiting nonlinear optical processes such as stimulated Raman–Stokes scattering (SRSS) [33,34]. Despite these endeavors, an efficient electrically driven laser is still quite elusive. As Ge PDs grown on silicon on insulator (SOI) became a standard process in Si photonics, research on light emitters using Ge flourished in the 2010s and was targeted on turning Ge into a direct bandgap semiconductor [35]. Lately, introducing Sn into Ge has been proven to be an effective method for obtaining a direct bandgap semiconductor. Both optically and electrically pumped GeSn lasers have been demonstrated recently [36,37]. There are several excellent review papers regarding building light sources using Group IV semiconductors and the readers can refer to these articles for more information [16,19–21,38]. In this section, we provide a brief review of the latest progress in Group-IV-based light sources on Si with an emphasis on the approaches adopted to achieve direct bandgap. We divide this section into three parts: Si-based light sources, Ge-based light sources, and GeSn-based light sources.

2.1. Si-Based Light Sources

Up to early 2000s, light emission from bulk Si, porous Si, and Si nano-crystals has been thoroughly explored [39–45]. The general idea is either to reduce non-radiative recombination through surface passivation and advanced doping [39,40] or to increase the luminescence efficiency via providing additional confinement for the charged carriers to improve the wave function overlap of the electron–hole pairs [41–45]. However, the emission wavelengths of Si-based light sources usually locate at the 1100 nm band for bulk Si and at the visible region for porous Si and Si nano-crystals, where Si itself manifests large absorptance. In addition, the light-emitting efficiency is quite low and an electrically driven laser has not been demonstrated.

Erbium-doped fiber amplifier (EDFA) has been the enabling technology for long-distance telecommunication. Analogously rare-earth atoms, especially erbium, can also be incorporated into Si as radiative recombination centers. Erbium-doped Si light sources emitting at the telecom 1.55 μm band can be readily integrated on-chip [46,47], with optical gain documented from erbium compounds [48]. Nevertheless, employing erbium doping to construct an on-chip light source for Si-photonics is still extremely challenging due to issues associated with long radiative lifetime, low power efficiency, and poor electrical carrier injection [20].

Another approach to achieve an all-Si light source involves the utilization of a phonon-assisted nonlinear optical process, where the energy of the pump laser is transferred to the Stokes beam via SRSS [49–53]. The first Si Raman laser was demonstrated in 2005 [34], and recently a widely tunable Si Raman laser with a tuning range of 83 nm and a power efficiency of 10% was reported [53]. Although Si Raman lasers are fully compatible with the existing CMOS process, it is inherently a wavelength-conversion process and still requires an external pumping laser source.

Figure 1

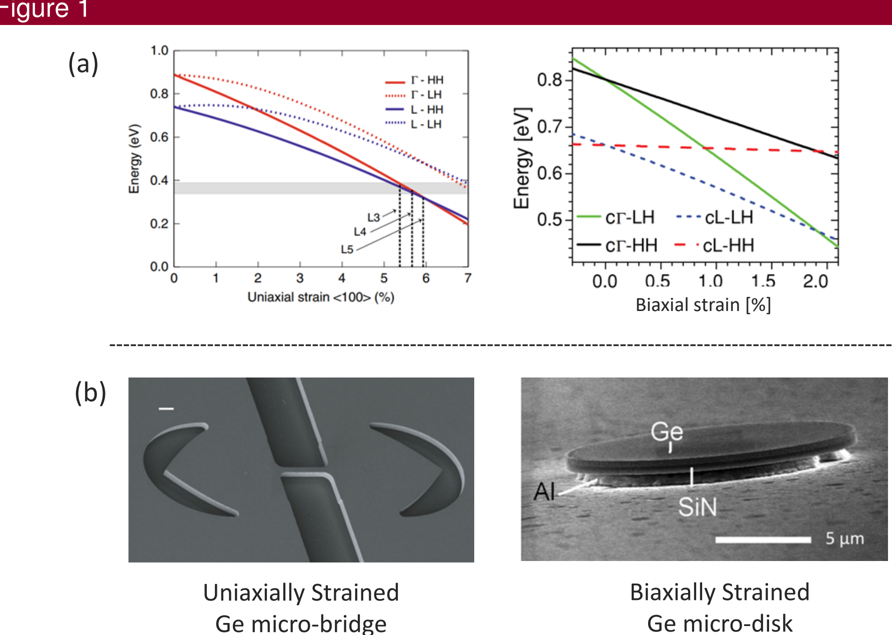

(a) Evolution of the band structure of Ge from indirect to direct when applying uniaxial and biaxial tensile strain. Reprinted from [56] under a Creative Commons license. (b) Lasers demonstrated from Ge micro-bridges and micro-disks using tensile strain. Reprinted from [56,58] under a Creative Commons license.

2.2. Ge-Based Light Sources

Despite the intensive efforts to obtain light emission from Si, finding a CMOS compatible semiconductor with a direct bandgap could significantly improve the light-emitting efficiency and shed light on the realization of electrically driven lasers. In contrast to Si with an energy separation of 2.28 eV between its X and Γ valley, Ge manifests a smaller energy difference of only 136 meV. More importantly, the band structure of Ge could be readily modified using strain [54]. In addition, Ge is also a CMOS-compatible material and is employed for building transistors with high hole mobility in Si-microelectronics as well as high-performance PDs in Si-photonics [38].

Applying tensile strain to Ge reduces the energy separation between the Γ and L valleys as well as the overall bandgap [35,55]. As indicated by the calculated plots in Fig. 1(a) [56,57], Ge is predicted to become a direct bandgap semiconductor when the uniaxial tensile stress approaches 6% or the biaxial stress exceeds 1.9% [58]. Uniaxial strain can be introduced via fabricating suspended Ge micro-bridges whereas biaxial strain could be created using stressor layers such as SiN as shown by the scanning electron microscopy (SEM) images in Fig. 1(b). Recently Pilon *et al.* demonstrated lasing from uniaxially strained Ge micro-bridges at 100 K [56], and Elbaz *et al.* reported lasing from biaxially strained Ge micro-disk lasers at 80 K [58]. Both devices emit in the mid-infrared region as the bandgap of Ge shrinks due to the applied tensile strain. The authors, however, argue that the strained Ge only marginally reaches direct bandgap and lasing can only be obtained at cryogenic temperatures when phonon-assisted valley scattering is negligible. Applying a higher strain would further shrink the bandgap and shift the emission wavelength into the longer mid-infrared region where room-temperature operation is commonly achieved by quantum/inter-band cascade lasers.

Apart from applying strain for direct bandgap, high n-doping could also greatly enhance the light-emitting efficiency of Ge. The donors could provide enough electrons

Figure 2

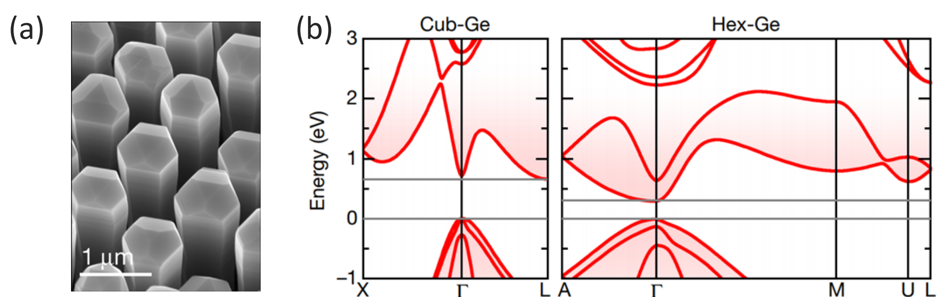

Hexagonal Si/Ge alloy with a direct bandgap. (a) SEM image of the hexagonal Si/Ge nanowire array. (b) Calculated band structure of cubic and hexagonal Ge. Reprinted by permission from Fadaly *et al.*, Nature **580**, 205–209 (2020) [66]. Copyright 2020 Springer Nature.

to fill up the L-valley minimum, and the injected electrons would, as a result, occupy the energy states in the Γ valley and recombine with holes radiatively. Combining tensile-strained Ge selectively grown on Si and heavy n-doping up to 10^{19} cm^{-3}, optically pumped Ge lasers were reported at room temperature under pulsed optical excitation [59]. Electrically driven devices were later demonstrated at 15°C under pulse injection condition [60]. However, an extremely large threshold current up to 280kA/cm^2 precludes practical application, and there have been no further reports of this approach, possibly due to the limited optical gain of Ge [61].

In addition to the radiative inter-band recombination, intra-band optical transitions within the conduction or the valance band can also be employed to build efficient light emitters, such as quantum cascade lasers (QCLs) [62]. SiGe/Si superlattices have enabled intra-band optical transitions within the valance band, and electroluminescence at 0.15 eV has been recorded from SiGe quantum cascade structures [63]. Investigation of this approach has been targeting at achieving efficient terahertz light emitters grown on Si substrates [64]. Another approach to obtain light emission from Ge involves the adoption of defect-enhanced Ge QDs. In this method, Ge ions are implanted into the self-assembled Ge QDs on Si substrates and the defect sites could significantly enhance light-emitting efficiency [65]. Although both cubic Si and Ge are indirect-bandgap semiconductors, Fadaly *et al.* recently reported that hexagonal Si/Ge alloys exhibit a direct bandgap and the emission wavelength can be tuned in a wide range in the mid-infrared regime through adjusting the composition of Si/Ge alloy [66]. Figure 2 shows the hexagonal Si/Ge nanowire array and the calculated band structure with a direct bandgap. This new finding elegantly resolves the issue of efficient direct bandgaps in Group IV semiconductors and might open a new venue for the research of Group IV light sources.

2.3. GeSn-Based Light Sources

As discussed in the previous section, the direct bandgap of a semiconductor is vital for the realization of efficient light emitters. In addition to mechanically introducing tensile strain to Ge, incorporating Sn into Ge matrix to form a GeSn alloy is another promising approach for obtaining a direct-bandgap Group IV semiconductor. Indeed, as indicated by Fig. 3(a), GeSn manifests a direct band structure when the Sn content exceeds 8% [36], and continues to increase with a higher Sn content. Similar to Ge, applying tensile strain to GeSn alloy could further increase the energy separation between the Γ and L minimum. This approach has attracted tremendous attention in the past few years and leads to the demonstration of both optically and electrically

Figure 3

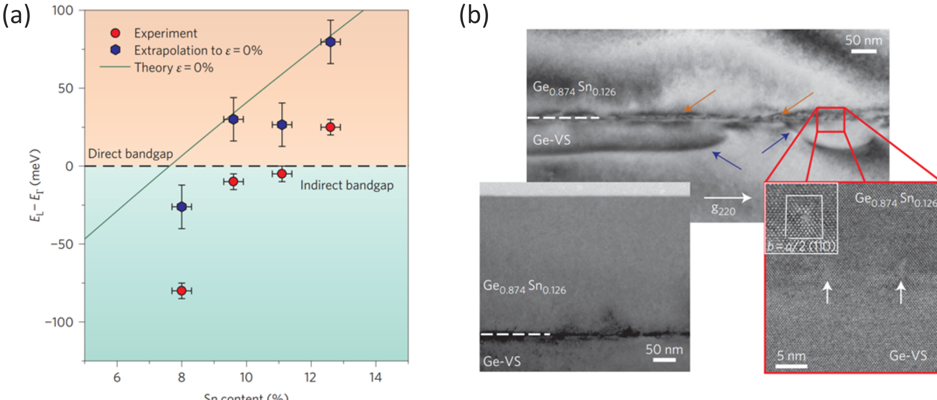

(a) Evolution of the energy separation between the Γ and L valley as a function of Sn content in Ge. (b) TEM images of GeSn alloy grown on Ge virtual substrate. Reprinted by permission from Wirths *et al.*, Nat. Photonics **9**, 88–92 (2015) [36]. Copyright 2015 Springer Nature.

pumped lasers on Si [36,37,67–74]. As expected, these GeSn light sources are often grown on virtual Ge/Si substrates (see Fig. 3(b)) and emit in the mid-infrared region. Efforts in this direction, as a result, target at potential applications in bio/chemical sensing, mid-infrared imaging, and spectroscopy.

2.3a. Optically Pumped GeSn Lasers

The first GeSn laser was demonstrated in 2015 via introducing 16% Sn into Ge and turning the GeSn alloy into a direct bandgap semiconductor [67]. The fabricated Fabry–Perot waveguide lasers can operate up to 90 K under pulse optical pumping. Afterwards, a higher Sn composition up to 20% was reported and lasing near room temperature was demonstrated, however, with a larger lasing threshold [68,69]. As the Sn content increases, the thermal stability of the GeSn alloy decreases as the equilibrium solubility of Sn in Ge is only around 1%. In addition, a higher Sn content in the GeSn alloy results in a larger lattice mismatch with the Ge/Si substrate and, thus, a higher defect density and resultant non-radiative recombination centers in the epitaxial GeSn alloy. Moreover, GeSn alloy with a larger Sn composition increases the built-in compressive strain, which unfortunately reduces the energy difference between the Γ and L valley and compromises the direct bandgap of the semiconductor.

A moderate Sn content could benefit GeSn light sources in terms of lower defect density and higher thermal stability. To obtain a direct bandgap from a GeSn alloy with a moderate Sn content, tensile strain can be applied using mechanical stressors such as building micro-bridges or depositing SiN cladding layers [70,71]. As presented in Fig. 4(a), Elbaz *et al.* demonstrated continuous-wave (cw) lasing from tensile-strained GeSn micro-disk lasers using SiN encapsulation layers. The devices feature a low threshold of 1.1 kW/cm^2 and could operate up to 70 K under cw optical pumping [72]. Apart from improving the band structure for efficient light emission, increasing the carrier confinement through constructing quantum structures could significantly benefit the device performance, as the historical evolution of III–V light sources unambiguously indicates. As shown by images in Fig. 4(b), Stange *et al.* utilized 22 nm GeSn quantum wells (QWs) with Sn content of 13.3% as the well layer and 22 nm SiGeSn alloy as the barrier to construct multi-quantum wells (MQWs) and to achieve strong confinement for both electrons and holes [73]. The relatively thick well is designed to maintain the direct bandgap of the GeSn compound as a thin well would

Figure 4

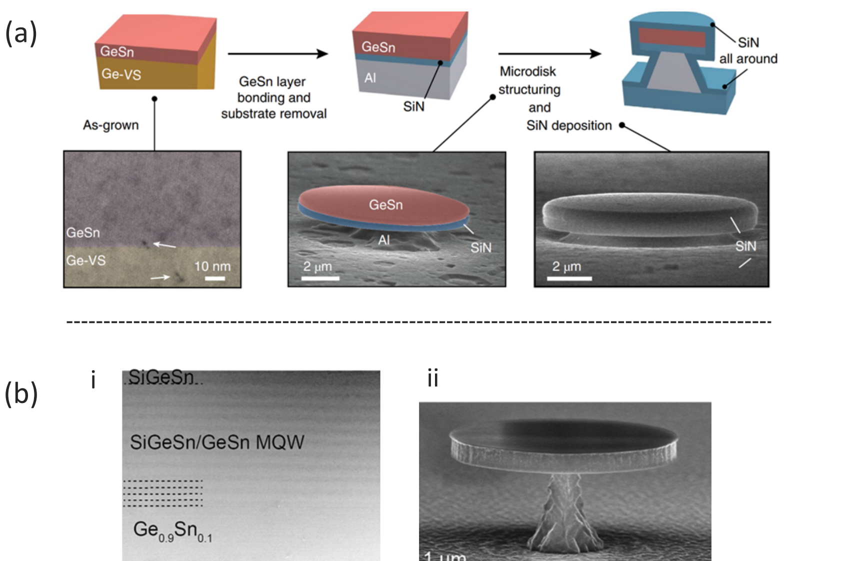

(a) Applying tensile strain to the indirect GeSn alloy using SiN stressor, achieving direct band structure and optically pumped GeSn micro-disk laser. Reprinted by permission from Elbaz *et al.*, Nat. Photonics **14**, 375–382 (2020) [72]. Copyright 2020 Springer Nature. (b) SiGeSn/GeSn MQWs for improved carrier confinement: (i) TEM image of the MQW; (ii) SEM image of an optically pumped MQW GeSn micro-disk laser. Reprinted with permission from Stange *et al.*, ACS Photonics **5**, 4628-4636 (2018) [73]. Copyright 2018 American Chemical Society, https://doi.org/10.1021/acsphotonics.8b01116.

have a larger compressive strain and thus reduced direct bandgap. Compared with lasers with bulk GeSn as the gain medium, devices with MQWs as a gain medium feature a 10 times reduction in lasing thresholds at 20 K and continue to outperform their bulk counterparts up to 100 K.

2.3b. Electrically Pumped GeSn Lasers

Unlike optically pumped lasers, constructing electrically driven devices entails a careful handling of issues regarding carrier injection and confinement, optical confinement, and metal-induced absorption loss. Recently, Zhou *et al.* demonstrated the first electrically injected GeSn lasers grown on Ge/Si substrates as shown in Figs. 5(a)–5(c) [37]. A GeSn/SiGeSn double heterostructure was selected to guarantee both carrier and optical confinement. A thin layer of p-SiGeSn was specially designed to circumvent hole leakage due to the type-II band alignment and facilitate hole injection into the active region. The fabricated ridge waveguide laser features a low threshold of 598 A/cm^2 at 10 K and can operate up to 100 K under pulsed electrical injection. The authors also reported a low external quantum efficiency (EQE) of only 0.3%. They attributed the small EQE to the small energy separation between the Γ and L valley, the insufficient carrier confinement from limited barrier height, and the large internal optical loss induced by crystalline defects in the active region.

The next breakthrough of Group-IV-based light sources would be the demonstration of an electrically driven cw laser operating at room temperature. Among the various strategies of Group IV light sources, GeSn lasers seem to be most promising approach, and continuing to modify the band structure of this semiconductor is of

Figure 5

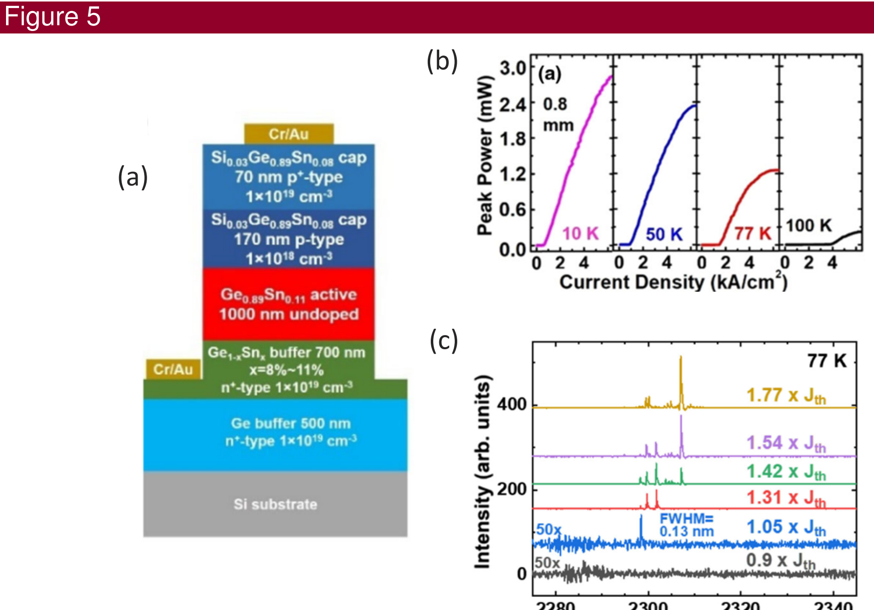

Electrically driven GeSn laser grown on Si. (a) Device structure of the electrically driven GeSn laser with a double heterostructure. (b) Evolution of the output power with the current density at different temperatures. (c) Emission spectra of the electrically driven laser at 77 K. Reprinted with permission from [37] © The Optical Society.

paramount importance. Even if this challenge is successfully tackled in the near future, GeSn-based light emitters would face the same challenges presently being extensively researched by the III–V on Si community. Examples include how to reduce the defect density of the epitaxial material for adequate device reliability and how to achieve efficient light coupling with Si-waveguides if a thick metamorphic buffer is mandatory for defect reduction. These issues will be discussed in detail in Sections 4 and 5, and the investigations of the III–V community might shed light on the future direction of GeSn light sources grown on Si.

3. HETEROGENEOUS INTEGRATION OF III-V LIGHT SOURCES ON SI

While there are plenty of exciting advances in the research of Group IV light sources in the past 20 years, an electrically driven laser emitter operating at room temperature has yet been demonstrated with Group IV gain regions. Current Si-based PICs in the market either adopt an off-chip III–V laser as the light source or incorporates an on-chip laser via heterogeneous integration [75,76]. Heterogenous integration, which has been sometimes interchangeably used with hybrid integration, refers to an integration scheme that transfers unprocessed non-Si materials or fabricated non-Si optoelectronic devices onto the Si-photonics wafer. In the case of integrating III–V light sources on Si, heterogeneous integration preserves the excellent optoelectronic properties of III–V gain materials grown on native substrates and, more importantly, guarantees an efficient on-chip light interfacing with Si waveguides. This feature combines the superior light emission/amplification of III–V compound semiconductors and the excellent waveguiding properties of Si and SiN. As a result, heterogeneous integration is currently the only commercially available technology and has enabled III–V light sources with unprecedented performance including cw electrically pumped lasers operating up to 150°C [3]. There are several excellent review articles on this topic in the past few years which the readers can refer to for more details [25,77–82]. In this section, we review the basics of two heterogeneous integration strategies: die/wafer

Figure 6

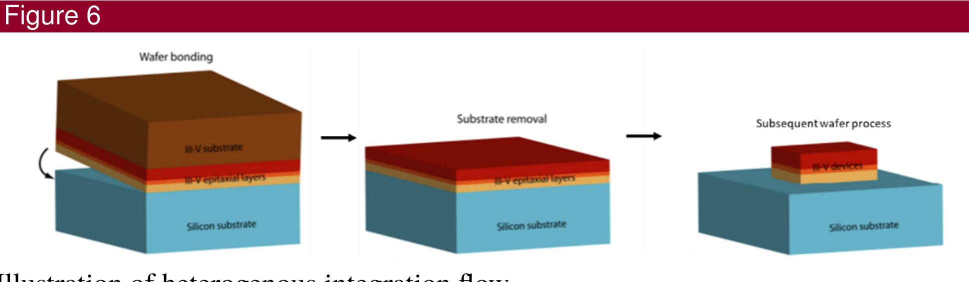

Illustration of heterogenous integration flow.

bonding and micro-transfer printing, highlighting the most recent progress in high performance III–V light sources that synergize the respective advantages of III–V and Si.

3.1. Die/Wafer Bonding

3.1a. Concept of Bonding

Die/wafer bonding is typically defined as an integration technique that transfers unprocessed non-Si material to a Si substrate, followed by conventional wafer level process to form fully integrated photonic circuits with both active and passive optical functionalities [83–89]. As the optical and electrical interfaces between light source and other active/passive devices are defined by lithography process which yields superior alignment accuracy over other mechanical alignment procedures, it provides great advantages in optical coupling efficiency as well as process scalability. Figure 6 illustrates a general heterogenous integration flow. The transfer of unprocessed non-Si material can be applied in various scales including wafer to wafer, partial wafer to wafer, or die to wafer, and the optimum size to use depends on overall process flow as well as economical trade-offs between of material cost and process complexity. In addition, it would be worthwhile noting that extensive engineering efforts have been made to bring this somewhat initially disruptive technology into the commercial silicon process facilities for commercialization. In particular, particle management throughout the process needs to be carefully carried out to achieve a good yield; this includes III–V chip singulation, III–V chip and wafer handling, and mechanical/chemical III–V substrate removal process steps.

The first electrically pumped heterogeneous laser on Si was demonstrated in 2006 [90] based on a hybrid waveguide structure as shown in Fig. 7. Figure 7(a) illustrates the overall waveguide architecture formed by the silicon waveguide and overlying III–V gain materials. Similar refractive indices of silicon and InP material systems enabled versatile waveguide engineering where the waveguide mode overlays both in the silicon waveguide and III–V QWs, and the amount of overlap in each region can be manipulated by changing the silicon waveguide width. As shown in Fig. 7(b), for example, the laser gain section can utilize the narrower silicon waveguide to maximize the optical gain by increasing the mode overlap to the III–V region, whereas the silicon waveguide width can be tapered wider at the coupling interface between the gain section and the silicon waveguide to ease the optical mode transition, which is typically facilitated further by horizontally tapering III–V mesa structure as well [91]. As this first demonstration was reported, various light source architectures using this Si heterogenous integration has been extensively researched and developed for various silicon photonics platforms that can be produced in large-scale silicon fabrication facilities [25,92–107]. In addition, recent demonstrations also showed that this technology can be extended to other low-loss broadband waveguide platform [108,109] as reviewed later in this section.

Figure 7

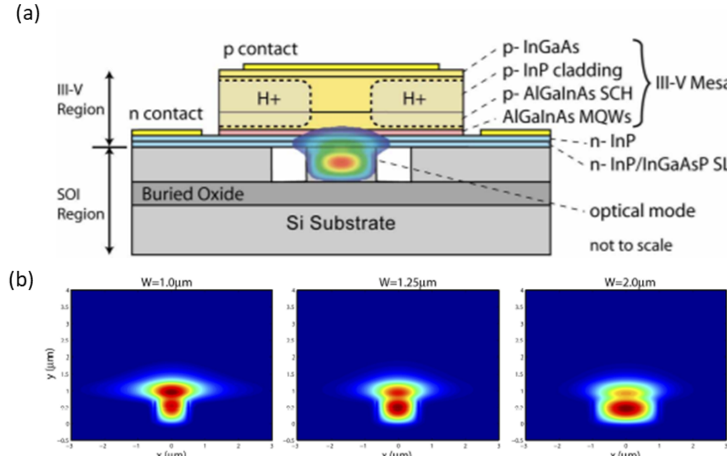

(a) Cross sectional structure of the first demonstrated InP–Si heterogeneous laser. (b) Simulated mode profile of the waveguide with various underlying silicon waveguide widths. Reprinted with permission from [90] © The Optical Society.

As a result of a continuous effort over a decade to bring III–V material and wafer bonding process into mainstream silicon manufacturing lines, this integration platform was first commercialized by Intel for pluggable optical transceivers both for parallel single-channel-based and wavelength division multiplex (WDM)-based architectures [3]. This milestone showcases that the heterogeneously integrated lasers can satisfy all the stringent requirements of optical transmitters both in performance and reliability aspects.

Figure 8(a) shows a schematic of the integrated CWDM transmitter with multiple heterogeneously integrated distributed feedback (DFB) lasers. The laser performance across the full O band shows a greater than 30mW at 80°C (Fig. 8(b)) and

Figure 8

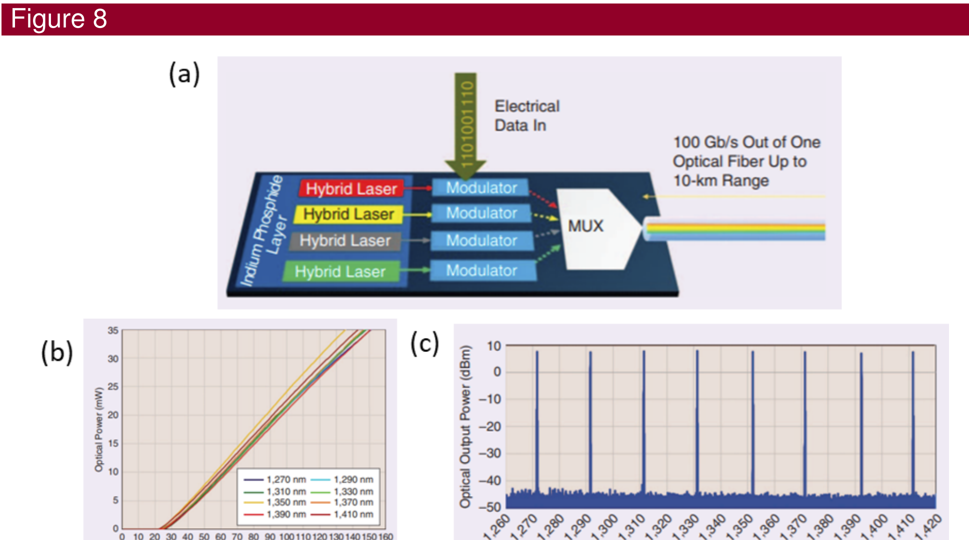

(a) CWDM transmitter schematic with multichannel heterogeneously integrated DFB lasers. (b) DFB LI characteristics at 80°C. (c) Overlaid lasing spectra from 8-channel DFB lasers. © 2019 IEEE. Reprinted, with permission, from Jones *et al.*, IEEE Nanotechnol. Mag. **13**, 17–26 (2019) [3].

Figure 9

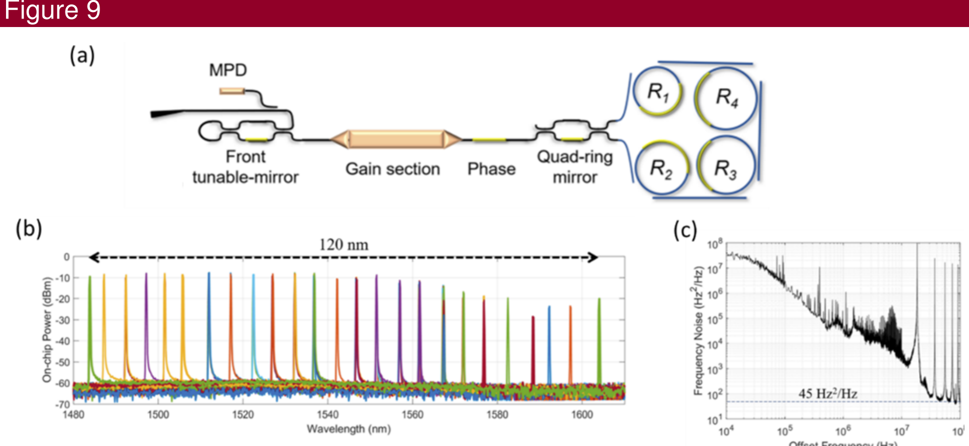

(a) Schematic of quad ring-based Si heterogenous tunable laser, (b) coarse tuning spectra over 120 nm, and (c) frequency noise spectrum. Reprinted from [115] under a Creative Commons license.

well-controlled lasing wavelength benefited from the 300 mm heterogeneous silicon process (Fig. 8(c)).

3.1b. High-Performance III–V/Si Light Sources

Although the first demonstrations and commercialization efforts have been primarily focused on optical transmitter applications, extensive research and development efforts over a past decade have also extended the potential application areas of heterogeneous photonic integration to non-communication fields such as augmented reality (AR)/virtual reality (VR), sensing, imaging, metrology and spectroscopy, and quantum-related technologies. A key advantage of the heterogenous approach is that it can integrate multiple material systems to fully utilize the best optical functionality from each material system into a single photonic integration circuit supported by a scalable and high-end wafer process. Recently widely tunable and narrow linewidth lasers are realized on Si heterogenous platform by combining optical gain from the heterogenous gain section and low-loss silicon waveguide-based ring resonators or Bragg gratings [110–114] and some of the performance metric exceeds those from lasers built on the native III–V substrates [115]. Figure 9 shows results from a recent demonstration of a widely tunable laser reported in Ref. [115]. The ring-resonator-based back mirror consists of four ring resonators with slightly different ring radii to increase Q and side mode suppression, and its effective cavity length is ~5 cm with a 0.18 dB/cm silicon waveguide loss. The quad ring design provided a good side mode suppression ratio between Vernier modes and resulted in a 120 nm tuning range as shown in Fig. 9(b). Figure 9(c) shows the frequency noise spectrum which exhibits a white noise level of 45 Hz^2/Hz starting at about 60–80 MHz frequency range. It corresponds to a Lorentzian linewidth of 140 Hz.

Silicon nitride (SiN) is another candidate for a passive waveguide material for heterogeneous integration, and features orders of magnitude lower waveguide loss compared with Si waveguides [108,116], with operating down to 400 nm wavelength regime [117]. For example, SiN-based ring resonators can yield an ultrahigh Q of greater than 160 million, and have been widely used in self-injection locked laser systems where they are typically butt-coupled with III–V native single-frequency lasers to reduce the Lorentzian linewidth by a factor of more than a million to just 0.04 Hz [109]. However, heterogeneous SiN integration still in early stage in developments compared with heterogeneous Si integration. This is primarily due to the difficulty

Figure 10

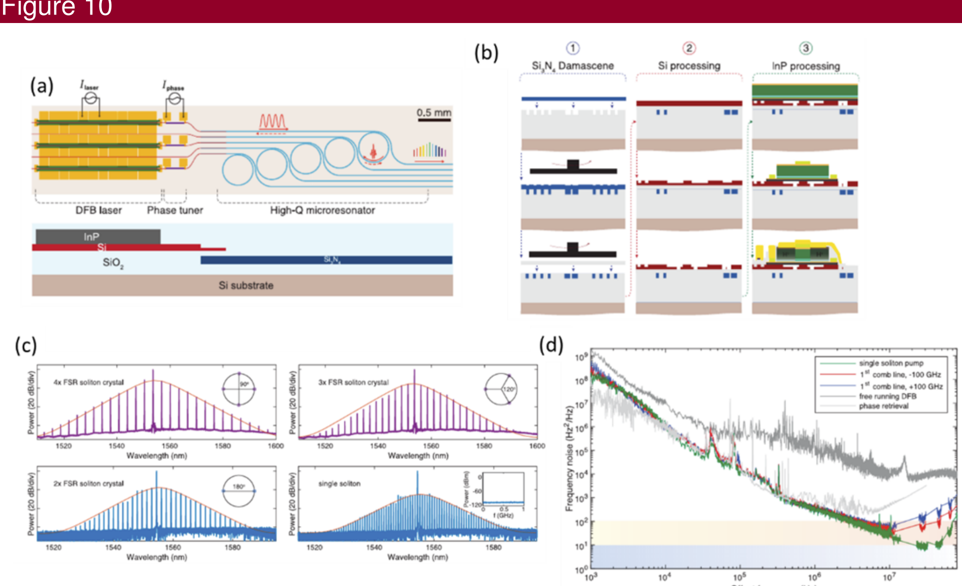

(a) Schematic of InP–Si–SiN heterogeneous chip scale laser soliton micro-comb. (b) Heterogeneous process flow. (c) Various soliton spectra with changing operating points. (d) Frequency noise spectra of the self-injection-locked pump line (green), comb lines with 100 GHz frequency offset to the pump (blue and red) in the single-soliton state, free-running single-mode DFB laser output without self-injection locking (dark gray), and comb line around 1550 nm for the two FSR soliton crystal state using optical phase retrieval method. From Xiang *et al.*, Science **2**, 99–113 (2021) [118]. Reprinted with permission from AAAS.

in achieving efficient optical coupling between the light source and the SiN passive waveguide, originating from a large difference in refractive indices between SiN and III–V material systems. The large index difference imposes a stringent requirement on the taper tip size if a typical adiabatic taper approach is chosen. Typically, this would require <50 nm taper tip size for efficient transmission without significant reflection. Given that the total thickness of III–V gain epitaxial layers typically reaches to 1–2 μm, formation of adiabatic tapers with small taper tip size imposes practical challenges in fabrication process. As an alternative approach to mitigate the challenges in direct optical coupling between III–V and SiN waveguides, multiple wafer bonding steps have been introduced to create InP-Si-SiN heterogeneous platform, where Si provides an intermediate waveguide layer to facilitate efficient optical coupling. Figures 10(a) and 10(b) show schematic and process flow of laser soliton micro-comb demonstrated by this approach [118]. A single-frequency pump laser is formed on the conventional Si heterogeneous laser structure and the output of the laser is coupled to silicon passive waveguide first. Then an adiabatic mode coupler on the silicon layer transfers the mode to the SiN micro-ring resonator. When the laser is injection locked by the SiN micro-resonator, soliton-based frequency comb is generated as shown in Fig. 10(c). From self-injection locking with the high-Q resonator, a great reduction of frequency noise has been also observed and Lorentzian linewidth of ~25 Hz was achieved on the pump frequency as shown in Fig. 10(d).

3.2. Micro-Transfer Printing

3.2a. Concept of Micro-Transfer Printing

In addition to die/wafer bonding, micro-transfer printing is another technique for heterogeneously integrating III–V light sources on mainstream Si-platforms. As indicated

Figure 11

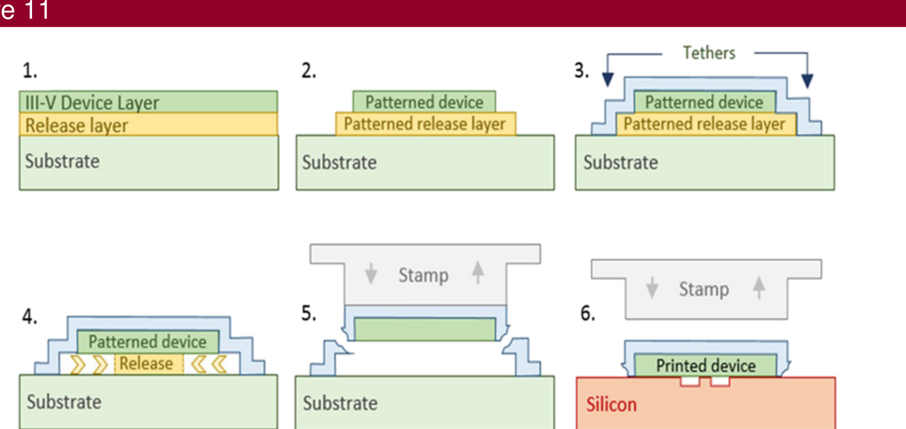

Process flow of micro-transfer printing. © 2018 IEEE. Reprinted, with permission, from Roelkens *et al.*, 2018 IEEE Optical Interconnects Conference (OI), pp. 13–14 (2018) [119].

by the schematics in Fig. 11, micro-transfer printing utilizes a polydimethylsiloxane (PDMS) stamp to pick-up arrays of pre-fabricated III–V devices, also referred to as coupons, from the III–V source substrate and then to transfer them onto the target Si wafer in a massively parallel manner [26,119,120]. The release of the coupons from the source substrate is enabled by undercutting the release layer beneath the device coupon and incorporating an encapsulation layer on top. As the adhesion strength of the coupons to the PDMS stamp depends on the peeling velocity of the stamp, the pick-up of the devices is obtained through setting a high peeling velocity and, thus, breaking the tethers to the source substrate. Similarly, the transfer of the coupons is achieved through setting a low retracting velocity and thus attaching the devices to the target Si wafer via van der Walls forces or an adhesive bonding agent [121,122]. As the PDMS stamp is transparent, alignment of the stamp to the coupons and subsequent Si-waveguides is attained via locating the codesigned fiducial markers on the source/target wafer using a pattern recognition function. The alignment accuracy is reported to be ±1.5 μm (3σ) when printed in large arrays and ±0.5 μm (3σ) when printed in small arrays [123]. This alignment accuracy via pattern recognition is lower than that of the die/wafer bonding approach using photolithography. Several previous reviews [26,124] contain a more comprehensive discussion of this integration approach.

Micro-transfer printing elegantly synergizes the conventional flip-chip integration approach and the die/wafer bonding scheme while possessing some of its own unique advantages. Similar to the flip-chip integration approach, micro-transfer printing enables the prefabrication and pretest of III–V light sources on the source substrate before being transferred to the target Si wafer and, as a result, necessitates no significant modification of the back-end process flow of the Si-photonics foundry. Akin to die/wafer bonding, micro-transfer printing allows for efficient light coupling between the heterogeneously-integrated III–V light sources and the Si-waveguides and subsequently produces a variety of advanced laser emitters. In contrast to flip-chip integration and wafer/die bonding, micro-transfer printing guarantees high-throughput integration due to the parallel printing style and a short printing cycle of just 30–45 seconds. In addition, micro-transfer printing could potentially reuse the expensive III–V source substrate and, thus, provide additional cost reduction. In principle micro-transfer printing could transport any coupons that can be released from the source substrate and, as a result, could enable the integration of a myriad of

Figure 12

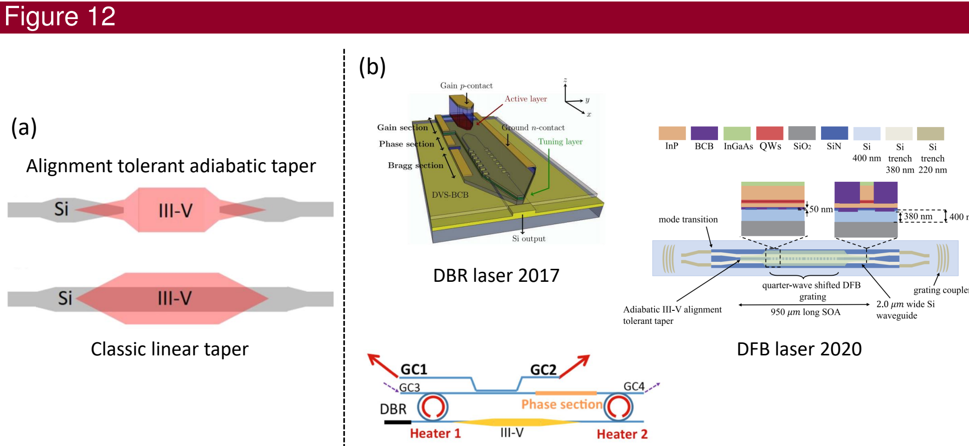

(a) Comparison of the alignment-tolerant adiabatic taper and the classic linear taper. Reprinted from [26] under a Creative Commons license. (b) Lasers with various cavities integrated on 400 nm SOI using evanescent coupling. Reprinted with permission from [112,129,130] © The Optical Society.

foreignoptoelectronics devices and even electronic driver circuits onto the mainstream Si-photonics platform [123].

3.2b. III–V-on-Si Light Sources

In the last few years, micro-transfer printing has been enabling the integration of III–V photodiodes, semiconductor optical amplifiers (SOAs), and laser diodes with various cavity designs onto the mainstream Si-photonics platforms [112,125–132]. Figure 12 summarizes recent progresses of III–V-on-Si light sources enabled by micro-transfer printing. In the initial proof-of-concept demonstration, a Fabry–Perot laser diode was transfer-printed into a recess on the 220 nm SOI platform, and light coupling with Si-waveguides is achieved via edge-coupling with a spot-size converter [128]. Although placing the III–V coupon atop the Si substrate is preferable for thermal dissipation, the alignment accuracy and the coupling uniformity require further improvement. To accommodate the relatively low alignment accuracy of micro-transfer printing, an adiabatic taper structure was specially designed to tolerate lateral misalignment up to 1.0 μm and thereby allows for efficient evanescent coupling with Si-waveguides on the 400 nm SOI platform as shown in Fig. 12(a) [26]. Building on this alignment-tolerant taper structure, advanced III–V-on Si laser emitters has been successfully demonstrated including distributed Bragg reflector (DBR) lasers [112], DFB lasers [129], and widely tunable lasers as indicated in Fig. 12(b) [130].

In addition to interfacing III–V lasers with Si-waveguides on the SOI platform, micro-transfer printing has also shown great potential for integrating III–V light sources onto the SiN platform. As the index contrast between III–V and SiN is significantly larger than that between III–V and Si, interfacing III–V gain materials with SiN waveguides has been challenging in the telecom band. Recently, de Beeck *et al.* overcame this obstacle through introducing hydrogenated amorphous silicon as an intermediate layer between III–V gain and the SiN and devising a two-step taper structure as shown by the schematic and the simulated mode profiles in Fig. 13(a) [131]. The authors then demonstrated heterogeneously integrated III–V SOAs and ring lasers on the SiN platform. Using a similar light coupling strategy, Cuyvers *et al.* reported a low noise III–V-on-SiN mode-locked laser via micro-transfer printing as indicated by the graph in Fig. 13(b) [132]. This heterogeneously integrated laser features a narrow line

Figure 13

(a)

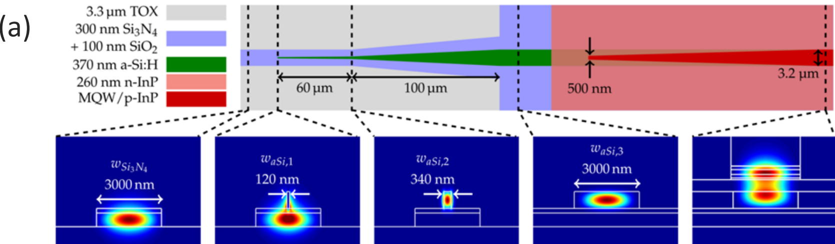

A two-step III-V/Si/SiN taper

(b)

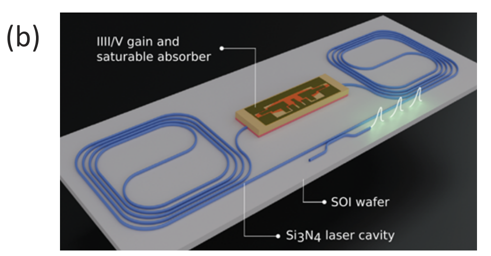

Mode locked lasers 2021

(c)

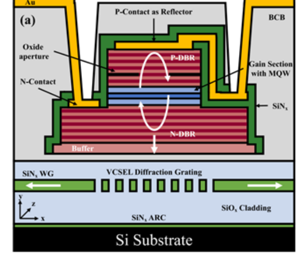

VCSELs 2021

(a) Design of a two-step III–V/Si/SiN taper structure. Reprinted with permission from [131] © The Optical Society. (b) III–V mode-locked lasers integrated onto SiN platform. Cuyvers *et al.*, Lasers Photonics Rev. 2000485 (2021) [132]. Copyright Wiley-VCH Verlag GmbH & Co. KGaA. Reproduced with permission. (c) VCSELs integrated onto SiN platform. Reprinted with permission from [133] © The Optical Society.

spacing of 755 MHz, a radio frequency linewidth of 1 Hz and an optical linewidth below 200 kHz. Recently vertical cavity surface emitting lasers (VCSELs) have also been integrated onto the SiN photonic platform using micro-transfer printing as shown in Fig. 13(c) [133].

4. BLANKET HETEROEPITAXY OF III-V LIGHT SOURCES ON SI

Compared with heterogeneous integration via bonding and micro-transfer printing, integrating III–V light sources on Si via direct heteroepitaxy is widely regarded as the ultimate monolithic solution that is scalable, low cost, and high throughput [20–22]. Directly depositing III–V thin films on large-scale Si wafers, also referred to as blanket heteroepitaxy, is the most straightforward approach and has been researched extensively in the past three decades [134–136]. As the laser designs and fabrication strategies resemble those of well-developed III–V photonics, investigation of this approach centers on how to grow device-quality III–V thin films on the mismatched Si substrate. Interestingly the investigation of growing III–V compounds on Si predates that of Si photonics. It was initially developed to combine the economical superiority of Si and the excellent optoelectronic properties of III–V compounds [137,138]. As Si and zinc-blende III–V manifest mismatches in lattice constant, coefficient of thermal expansion and polarity, direct growth of III–V thin films on Si wafers has been challenging. The lattice and thermal mismatches result in a high density of TDs while the polarity mismatch gives rise to anti-phase boundaries (APBs) with electrically charged III–III and V–V bonds. These crystalline defects serve as non-radiative recombination centers and current leakage sources that severely impact the performance of III–V optoelectronics devices. This issue is especially fatal in III–V lasers grown on Si as the defects move and multiply into dark line defects (DLD)

under high current injection conditions, which lead to early device failure [139]. As a result, the key to integrating III–V lasers on Si via blanket heteroepitaxy lies at designing epitaxial techniques to reduce the density of TDs and eliminate APBs. As conventional MQWs are particularly susceptible to the influence of TDs, employing TD-insensitive quantum structures such as QDs and quantum dashes as the active gain medium improves the reliability of III–V lasers directly grown on Si [140]. In this section, we review the latest advances in growing III–V lasers on Si using blanket heteroepitaxy with an emphasis on the different defect-management techniques. We divide this section into three parts: GaAs-based QD lasers emitting in the 1.3 μm band, InP-based lasers emitting in the 1.55 μm band, and GaSb-based lasers emitting in the mid-infrared region.

4.1. GaAs-Based Light Sources

4.1a. GaAs Thin Films Grown on Si

GaAs has long been the primary material for light sources emitting in the near-infrared band, and efforts in directly growing GaAs thin films on Si dates back to the early 1980s [136,137]. In these earlier investigations, Si wafers with an offcut angle of 4°–6° were often adopted to eliminate the formation of APBs, and a Ge buffer layer was frequently employed to bridge the 4% lattice mismatch between GaAs and Si [135,136]. As the Si industry uses on-axis (001) Si wafers without large offcut angles and Ge layer absorbs light in the telecom band, new growth techniques are being developed to directly grow GaAs thin films on (001) Si wafers or substrates with offcut angles less than 0.5°. However, exact (001)-oriented Si surface often features single atomic steps and facilitates the formation of APBs, special growth techniques must be designed to deposit APB-free GaAs thin films. Through careful surface treatment such as annealing the Si substrate at high temperature prior to GaAs deposition, the density of APB formed at the GaAs/Si interface can be reduced and the APBs can be completely self-annihilated within a thin layer of GaAs buffer (see Fig. 14(a)) [141,142]. Another approach shown in Fig. 14(b) uses GaP as an intermediate layer for the subsequent GaAs growth, and APBs can be eliminated within the 100-nm-thick GaP layer [143]. Currently 300 mm GaP/Si templates are commercially available by $NAsP_{III-V}$. In contrast to (001) Si surface with single atomic steps, (111)-oriented Si facets inherently feature double atomic steps and, thus, could effectively preclude the formation of APBs [146]. As shown by the schematic and TEM images in Fig. 14(c), patterned (001) Si substrates with (111)-oriented V-grooves can produce APB-free GaAs thin films on exact (001) Si wafers. In this scenario, GaAs nano-ridges first form inside the V- grooves and then coalesce together into continuous GaAs thin films [144].

APBs can be readily removed using these novel growth methods, but the epitaxial GaAs thin films still manifest a TD density up to 10^9 cm^{-2}. Figure 15 lists three major TD management approaches: strained layer superlattice (SLS), thermal cycle annealing (TCA), and misfit trapping layers. Employing SLS and TCA, the TD density of current GaAs/Si templates have been reduced to the order of 10^6 cm^{-2} [147,148]. Recent research indicates that insertion of misfit trapping layers below and above the active region can prevent the formation of misfit dislocations in the active gain medium and, thus, further reduce the influence of TDs on device performance. This technique has been proven to be vital for reliably operating lasers at high temperatures [149]. Note that these TD filtering methods are also applicable for the growth of InP and GaSb thin films on Si.

4.1b. 1.3 μm QD Lasers on GaAs/Si Templates

In addition to reducing the TD density of GaAs/Si templates, the adoption of InAs QDs as the active gain medium is another essential factor for the success of GaAs-based QD

Figure 14

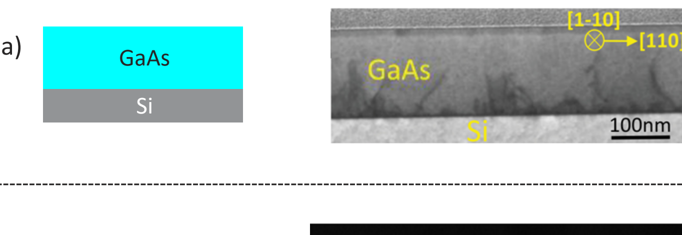

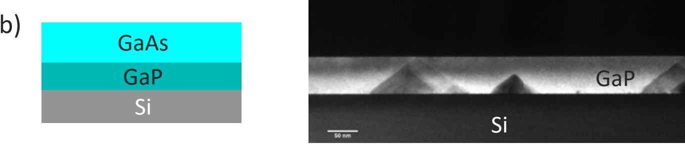

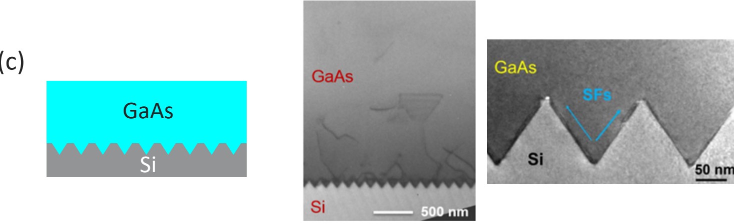

Blanket heteroepitaxy of GaAs thin films on (001) Si substrates. (a) GaAs thin film directly grown on Si with careful surface treatment. Reprinted with permission from Martin *et al.*, Appl. Phys. Lett. **109**, 253103 (2016) [141]. Copyright 2016, AIP Publishing LLC. (b) GaAs thin film grown on Si with a thin GaP intermediate layer. Reprinted from Volz *et al.*, J. Crystal Growth. **315**, 37–47 (2011) [143], with permission from Elsevier. (c) GaAs thin film grown on V-grooved patterned Si. Reprinted with permission from Wan *et al.*, Appl. Phys. Lett. **108**, 221101 (2016) [145]. Copyright 2016, AIP Publishing LLC.

Figure 15

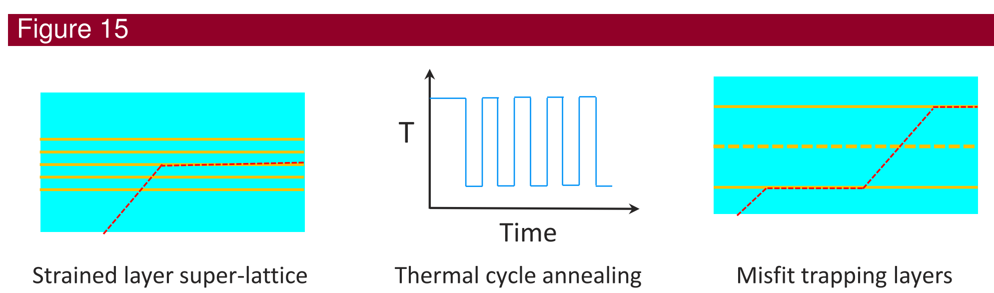

Current techniques adopted to further reduce the TD density in the epitaxial III–V thin film on Si.

lasers grown on Si. Apart from emission in the telecom 1.3 µm band, InAs QDs with delta function-like density of states and strong three-dimensional carrier confinement are significantly less susceptible to the influence of TDs compared with conventional QWs [140]. In addition, QDs benefit light sources in terms of low transparency current density, isolator-free operation, and high-temperature operation [150]. In the last few years, there has been a variety of GaAs-based 1.3 µm QD lasers directly grown on (001) Si wafers as schematically summarized in Fig. 16 [140,145,151–159]. Examples include, but are not limited to, Fabry–Perot lasers, micro-disk/ring lasers, photonic crystal cavity (PhC) lasers, DFB lasers, tunable lasers, and mode-locked lasers. The reader can refer to previous review articles for detailed discussions [28,160–166].

Figure 16

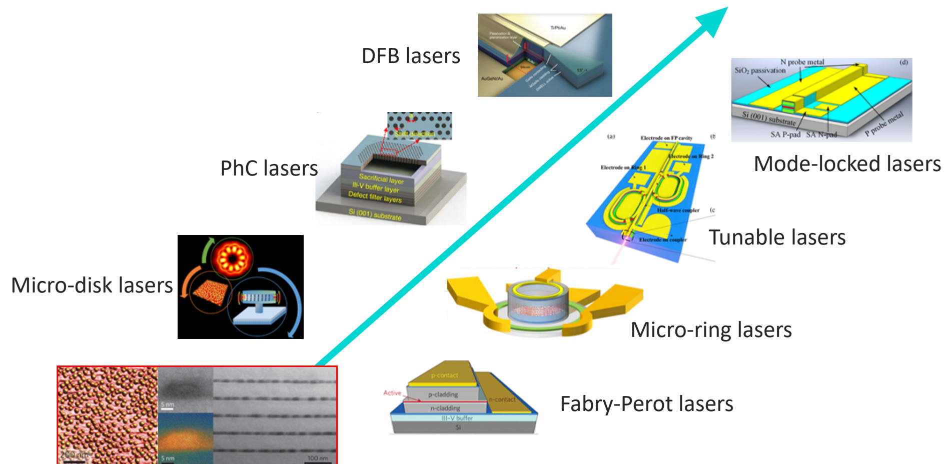

A variety of GaAs-based 1.3 μm QD lasers directly grown on (001) Si substrate. Reprinted by permission from Springer Nature, Chen *et al.*, Nat. Photonics. **10**, 307 (2016) [140], copyright 2016. Reprinted with permission from Wan *et al.*, Applied Phys. Lett. **108**, 221101 (2016) [145]. Copyright 2016, AIP Publishing LLC. Reprinted from [154] under a Creative Commons license. Reprinted with permission from [151–153,155–159] © The Optical Society.

Apart from 1.3 μm InAs QDs, GaAs can also serve as buffer layers for the growth of red-emitting InP QDs [167,168]. In addition, InP QD laser diodes directly grown on GaAs/Si templates have been demonstrated recently [169].

Operating lasers grown on Si reliably in high-temperature ambient is vital for the commercial success of this technology. As shown by the plots in Fig. 17, using GaAs template with a TD density of 1×10^{6} cm^{-2} and embedded misfit trapping layers, 1.3 μm QD lasers have been proven to exhibit an extrapolated lifetime of over 10 years under an operating temperature of 80°C as well as a low threshold current density of 266 A/cm^2 [149]. This demonstration marks an important step toward the commercial success of this technology by Quintessent and others and highlights the great potential of integrating III–V light sources on Si using direct heteroepitaxy.

4.2. InP-Based Light Sources

4.2a. InP Thin Films Grown on Si

Although GaAs-based lasers can emit light in the telecom 1.3 μm band using InAs QDs as active gain medium, constructing lasers emitting in the entire telecom band especially in the 1.55 μm band necessitates InP and its related compounds. InP is a photonic integration platform on its own and has dominated telecom applications for decades [30]. However, due to the large lattice mismatch, up to 8% between InP and Si, it is extremely challenging to directly grow InP thin films on Si with low TD density. In addition, the diffusive characteristics of indium adatoms often result in a rough crystal surface, further complicating subsequent device implementation [170]. As the lattice constant of GaAs falls between InP and Si, the most straightforward and widely adopted approach to deposit InP thin films on Si involves using GaAs as an intermediate layer [171,172]. As shown by the schematics and TEM images in Figs. 18(a) and 18(b), InP thin films can be directly deposited atop the GaAs/Si template using a conventional two-step growth procedure consisting of low-temperature nucleation and high-temperature main layer [172], and graded InGaAs buffer layers can also be

Figure 17

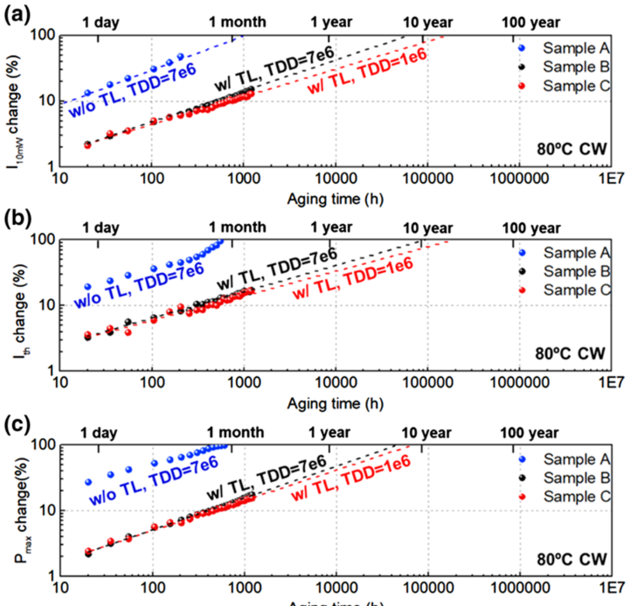

Aging test of GaAs-based QD lasers directly grown on Si, showing an extrapolated lifetime of over 10 years under 80°C cw operation. Reprinted with permission from [149] © The Optical Society.

employed to bridge the lattice between GaAs and InP [170]. Directly depositing InP thin films on Si substrates has also been proven feasible through using patterned Si substrate with V-grooves as illustrated in Fig. 18(c) [173]. Although the V-grooves prevent the formation of APBs, this approach often results in the formation of a high density of stacking faults (SFs) penetrating toward the InP surface. TD management techniques, such as SLS and TCA, are also applicable for InP thin films grown on Si. Currently the TD density of InP thin films grown on Si is of the order of 10^8 cm^{-2}, still two orders magnitude larger than that of GaAs thin films on Si.

4.2b. 1.55 µm Lasers on InP/Si Templates

Although GaAs-based MQW lasers grown on Si have been widely regarded as unpractical due to DLD-induced early device failures, this issue has been proven to be significantly less severe for InP-based MQW devices [146,174]. This is because the defect states induced by dangling bonds lies closer to the mid-gap in GaAs than that in InP, and the non-radiative recombination rate and resultant dislocation motion is much server in GaAs than that in InP [175]. Shi *et al.* demonstrated room-temperature cw lasing through employing InGaAsP MQWs as the active gain medium as shown in Fig. 19(a) [176]. The Fabry–Perot lasers feature a threshold current density of 2.05 kA/cm^2 and can operate up to 65°C. Although these devices can stably operate over 200 hours at 10°C under cw driving, they manifest a rapid device failure at 60°C after just 5.6 hours of aging under pulsed operation [181]. This observation highlights the necessity of further reducing the TD density of the InP/Si templates. Apart from InGaAsP QWs, InAs quantum dashes and QDs have also been chosen as the active gain medium for light sources emitting in the 1.55 µm band. In contrast to InAs deposited on (001) GaAs surface where ensembles of dots can be readily formed, depositing InAs on (001) InP surface often results in elongated dashes or dots with a large diameter-to-height ratio [182]. Figure 19(b) displays an atomic force microscopy (AFM) image of InAs quantum dashes grown on an InP/Si template. Employing the InAs quantum dash as the active gain medium, Lin *et al.* reported room-temperature micro-disk lasers

Figure 18

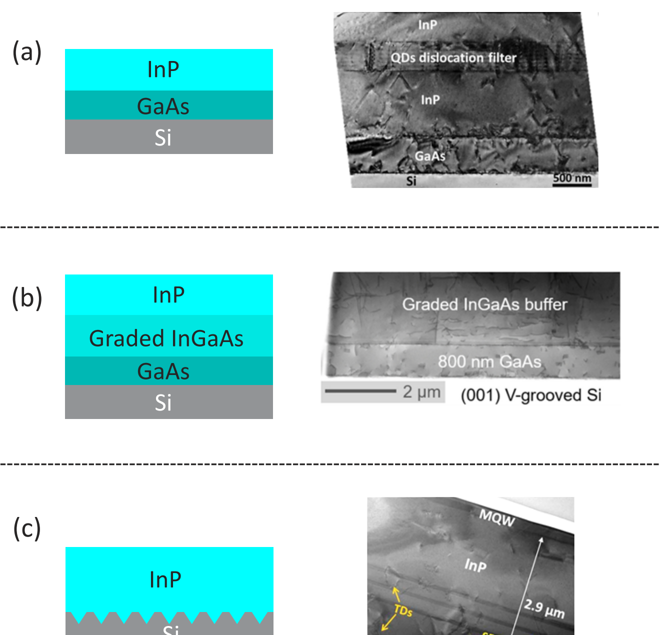

Blanket heteroepitaxy of InP thin films on (001) Si substrates. (a) InP thin film directly grown on Si with a thick GaAs intermediate layer. Reprinted with permission from Shi *et al.*, ACS Photonics. **4**, 204–210 (2017) [172]. Copyright 2017 American Chemical Society, https://doi.org/10.1021/acs.6b00731. (b) InP thin film grown on Si with thick InGaAs graded buffer and GaAs intermediate layer. Reprinted with permission from Shi *et al.*, J. Appl. Phys. **127**, 033102 (2020) [170]. Copyright 2020, AIP Publishing LLC. (c) InP thin film directly grown on V-grooved patterned Si. © 2015 IEEE. Reprinted, with permission, from Shi *et al.*, IEEE Photonics Technol. Lett. **27**, 748–751 (2015) [173].

under cw pumping [177]; Xue *et al.* demonstrated Fabry–Perot laser diodes with a threshold current density of 1.3 kA/cm^2 and cw operation up to 59°C [178]. Figure 19 (c) presents an AFM image of InAs QDs grown on an InP/Si template. Utilizing these QDs as the active gain medium, Shi *et al.* reported room-temperature micro-disk lasers under pulsed excitation [179]; Zhu *et al.* demonstrated Fabry–Perot laser diodes with a threshold current density of 1.6 kA/cm^2 and operation up to 80°C under pulsed driving conditions [180]. Note that the optical property of quantum dashes in Ref. [178] is superior compared with QDs in Ref. [180] grown on (001) InP/Si complaint substrates, which might partly account for the cw operation of quantum dash lasers on Si.

4.3. GaSb-Based Light Sources

4.3a. GaSb Thin Films Grown on Si

GaSb and its 0.61 nm lattice constant family compounds have been the enabling material system for light sources and detectors in the mid-infrared region [183]. With a lattice mismatch up to 12% between GaSb and Si, research of growing GaSb thin films on Si wafers used to be quite scarce [184–188], and earlier efforts focused on depositing GaSb thin films on GaAs substrate instead [189]. Interestingly directly growing GaSb thin films on GaAs substrates leads to the formation of interfacial misfit (IMF) array: a two-dimensional misfit dislocation network. This IMF array could release strain

Figure 19

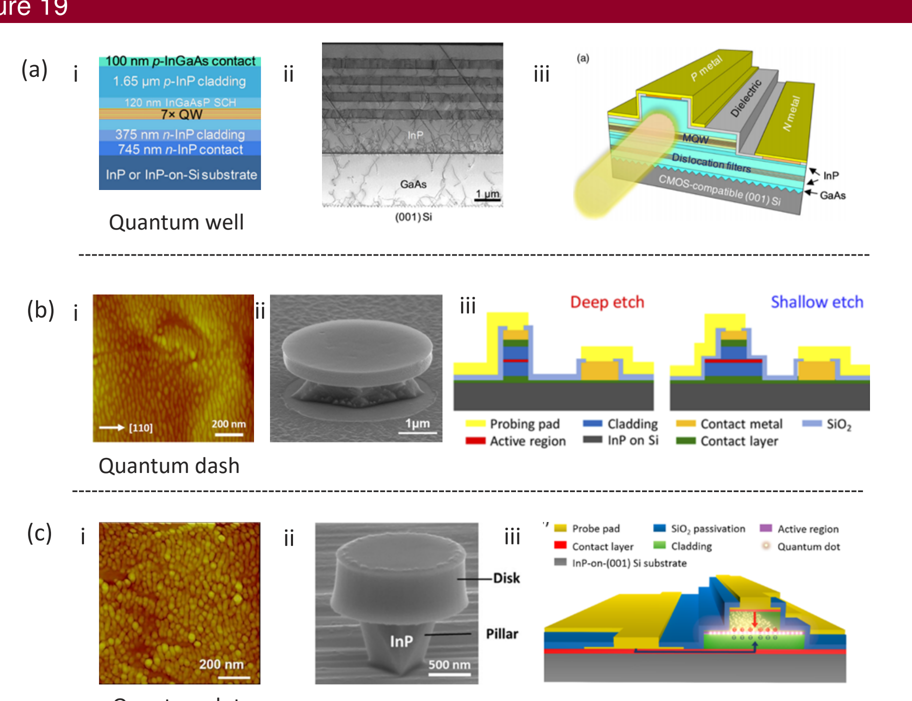

(a) InP-based 1.55 µm QW diode lasers grown on (001) Si substrate. Reprinted with permission from [176] © The Optical Society. (b) InP-based 1.55 µm quantum dash micro-disk and diode lasers grown on (001) Si substrate. Reprinted with permission from [177,178] © The Optical Society. (c) InP-based 1.55 µm QD micro-disk and diode lasers grown on (001) Si substrate. Reprinted with permission from Shi *et al.*, Appl. Phys. Lett. **110**, 121109 (2017) [179]. Copyright 2017, AIP Publishing LLC. Reprinted with permission from Zhu *et al.*, Appl. Phys. Lett. **113**, 221103 (2018) [180]. Copyright 2018, AIP Publishing LLC.

within a thin layer of GaSb as evidenced by the TEM images in Fig. 20(a) [189]. As the research on mid-infrared Si-photonics flourished in recent years, there has been a growing need to monolithically integrate GaSb-based light sources onto the mainstream Si platform. Similar to the case of InP thin films on Si, GaSb thin films on Si can be created through depositing GaSb atop the optimized GaAs/Si templates as schematically shown in Fig. 20(a) [188]. Recent research indicates that it is also possible to directly grow high-quality GaSb thin films on exact (001) Si substrates without any lattice bridging layers. As evidenced by the schematic and the TEM image in Fig. 20(b), researchers reported GaSb thin films on Si with a TD density less than 8.5×10^7 cm^{-2} [190]. Although APBs appear at the initial stage of GaSb growth, they gradually self-annihilate as the buffer layer thickens. The aforementioned epitaxial method using patterned Si substrates with V-grooves can also be applied for the growth of GaSb and InAs thin films on Si [187]. As shown by the TEM image in Fig. 20(c), the air voids formed during the coalescence of GaSb nano-ridges function as defect-trapping free surfaces and prevent the propagation of SFs into the GaSb thin films above.

4.3b. Mid-Infrared Lasers on GaSb/Si Templates

Unlike the case of GaAs- and InP-based telecom light sources grown on Si where plenty of demonstrations are available in the literature, reports of GaSb-based mid-infrared light sources grown on Si are relatively limited [190–195]. Recently, Rio Calvo *et al*

Figure 20

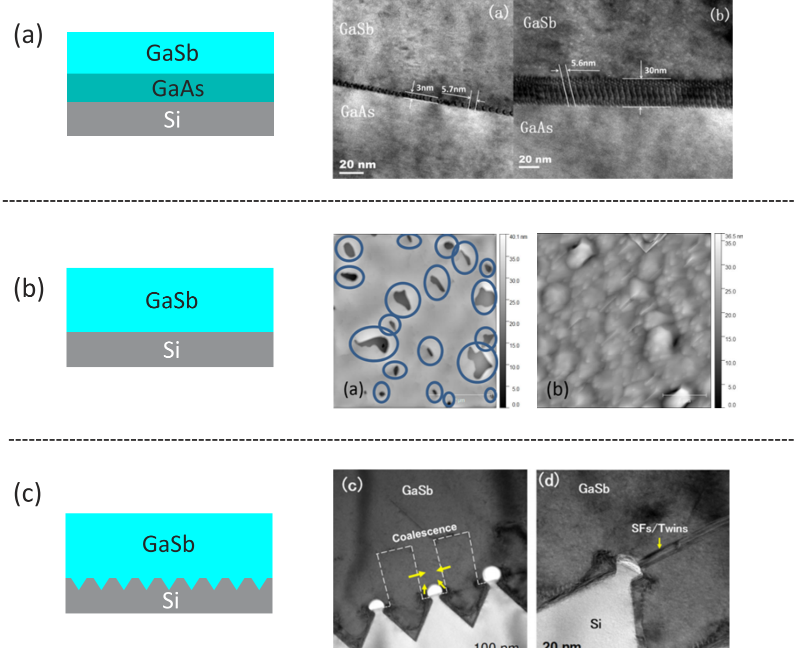

Blanket heteroepitaxy of GaSb thin films on (001) Si substrates. (a) GaSb thin film grown on Si with GaAs intermediate layer. Reprinted with permission from Zhou *et al.*, Appl. Phys. Lett. **99**, 221917 (2011) [189]. Copyright 2011, AIP Publishing LLC. (b) GaSb thin film directly grown on Si. Reprinted with permission from [190] © The Optical Society. (c) GaSb thin film directly grown on V-grooved patterned Si substrates [187]. Reprinted with permission from Li *et al.*, Appl. Phys. Lett. **111**, 172103 (2017) [189]. Copyright 2017, AIP Publishing LLC.

al. demonstrated high-performance mid-infrared GaSb-based laser diodes integrated on (001) Si using blanket heteroepitaxy [190]. The active region consists of two GaInAlSb/AlGaAsSb QWs, and the devices feature a low threshold current density of 400–500 A/cm^2 and can operate up to 80°C under cw driving without noticeable thermal rollover. The GaSb/Si templates can also be employed to construct QCLs and interband cascade lasers (ICLs) [194,195]. Recently Cerutti *et al.* reported InGaSb/InAs ICLs directly grown on Si with a similar device performance to those grown on native GaSb substrates [195]. Despite a TD density over 10^8 cm^2, these devices exhibit an extrapolated mean time to failure over 312,000 hours as shown by the plots in Fig. 21(b). This impressive result is achieved through designing a type-II band alignment that renders QW lasers highly tolerant to dislocations as schematically indicated in Fig. 21(a). In this scenario, the non-radiative recombination via trap levels is suppressed significantly.

Although GaAs-based 1.3 μm QD lasers grown on Si are rapidly maturing toward commercialization, the InP-based 1.55 μm and GaSb-based mid-infrared light sources grown on Si are still under intense academic investigation. Research targets at reducing the TD density of the InP/Si and GaSb/Si templates from the current order of 10^8 cm^{-2} to the future order of 10^6 cm^{-2}. However, this is by no means a trivial task as their lattice mismatch with Si are significantly larger than that between GaAs and Si. New growth strategies and defect management techniques are required to further reduce the TD density of the epitaxial III–V thin films. For III–V light sources integrated on Si by blanket heteroepitaxy, a buffer layer with a thickness of a few micrometers

Figure 21

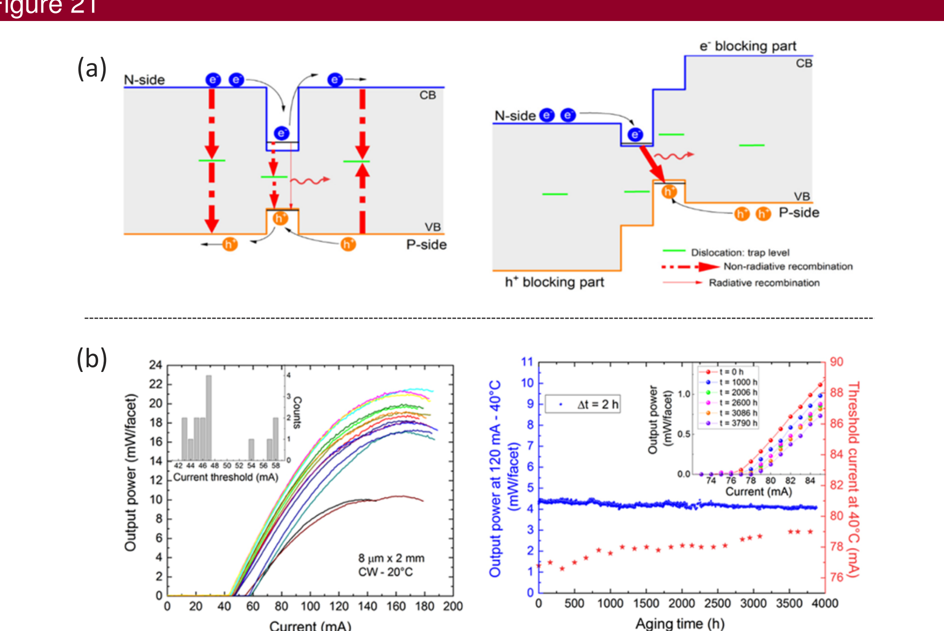

(a), (b) Mid-infrared GaSb-based ICLs grown on Si that are highly tolerant to dislocations. Reprinted with permission from [195] © The Optical Society.

is required for defect reduction. These thick buffers make it extremely challenging to couple light from the above III–V laser diodes into the Si-waveguides underneath. Several approaches have been proposed and theoretically verified to tackle this issue [28,196,197]. Experimental demonstrations, however, are not yet available.

5. SELECTIVE HETEROEPITAXY OF III-V LIGHT SOURCES ON SI

Although blanket heteroepitaxy has yielded high-performance III–V diode lasers on Si wafers, future integration with Si-based passive optical components requires selective growth of these lasers at pre-defined areas on Si substrates as well as the efficient light coupling with Si-waveguides. Selective heteroepitaxy of III–V lasers on Si brings about additional advantages unavailable in conventional blanket heteroepitaxy utilizing the inherent defect necking effect in areas with large aspect ratio [198]. First, localized growth results in the confinement of inclined crystal defects including TDs and SFs and accordingly enables the growth of TD-free III–V materials on Si, which is crucial for the reliability of lasers grown on Si [199]. Second, this unique defect reduction mechanism eases the issue of lattice mismatch between III–V and Si, and therefore allows for the epitaxy and even co-epitaxy of a variety of III–V alloys on Si such as GaAs, InP, GaSb and InAs [29,200–207]. Third, crystal growth in selective heteroepitaxy is often guided by the patterned oxide mask, which enables the epitaxy of III–V crystals with different directions, phases, and geometries [208,209]. Fourth, unlike blanket heteroepitaxy where buffer layers with a thickness of a few micrometers are mandatory for defect reduction, selective heteroepitaxy confines the defective portion of the epitaxial material right at the III–V/Si interface or within a few tens of nanometer of interfacial layer. Such a "bufferless" feature results in the close placement of the epitaxial III–V layer and the Si device layer and consequently enables efficient on-chip light coupling between III–V light sources and Si-waveguides [210]. In this section, we review the most recent progress of integrating III–V light sources on Si via four different selective heteroepitaxy schemes. We start with introducing the basic concept of each scheme and then discuss the latest demonstrations of optically

Figure 22

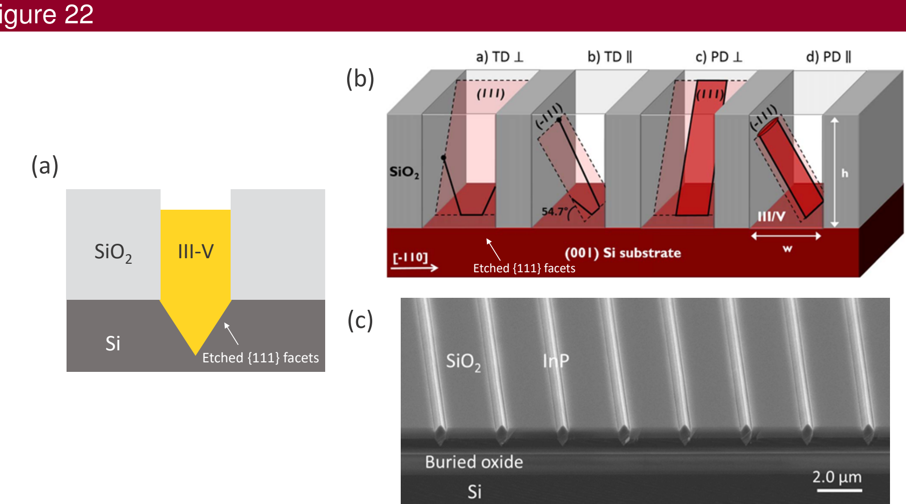

Basic concept of the ART growth scheme. (a) Schematic of III–V nano-ridges grown on V-grooved Si pockets. (b) Unique defect necking effect of the ART growth scheme. Reprinted with permission from Kunert *et al.*, Semicond. Sci. Technol. **33**, 093002 (2018) [198], https://doi.org/10.1088/1361-6641/aad655. © IOP Publishing. Reproduced with permission. All rights reserved. (c) SEM image of in-plane InP nano-ridges grown on SOI wafers using ART.

pumped lasers selectively grown on Si. We conclude each part with a brief perspective on the approaches to attain efficient light coupling into Si waveguides and proposed strategies to achieve electrically driven lasers selectively grown on Si.

5.1. Vertical Integration Schemes

5.1a. Aspect Ratio Trapping

As shown by the schematic in Fig. 22(a), the aspect ratio trapping (ART) scheme refers to the selective area growth of vertical III–V nano-ridges inside V-grooved trenches enclosed by two oxide spacers. These trenches usually run along the [110] direction, and the V-grooves with two {111} Si facets are created using anisotropic wet etching (KOH or TMMA). The generated crystal defects from lattice mismatch are accordingly trapped by the oxide sidewall [136,198]. Initiating III–V nucleation from the {111}-oriented Si facets precludes the formation of APBs. As depicted schematically in Fig. 22(b), any TDs gliding along the {111} planes will be trapped by the oxide spacers and the epitaxial III–V crystal is presumably TD-free when the aspect ratio of the trench (height over width) is larger than 1.4 [198]. SFs parallel to the trench will also be trapped by the oxide spacers while those perpendicular to the trench direction cannot be trapped and will run through the entire epitaxial III–V nano-ridge. However, in contrast to blanket heteroepitaxy where SFs are accompanied by two partial TDs, these SFs inside III–V nano-ridges extend across the entire crystal and terminate at the oxide spacer walls, and thereby under no circumstances introduce any partial TDs inside the crystal [198,211]. Initially developed for III–V electronic devices for advanced logic applications [212–215], this ART strategy has recently been deployed to integrate III–V light sources on mainstream Si platform [216]. Figure 22(c) displays an example of InP nano-ridge array selectively grown on (001) SOI wafers for laser array emitting in the 1.5 µm band.

To build lasers from III–V nano-ridges grown on Si, a few factors must be carefully managed. First, the dimension of the nano-ridge is often set around a few hundred nanometers to attain a delicate balance between the effective defect necking effect and the efficient waveguiding in the near infrared range. A wider nano-ridge results in a

Figure 23

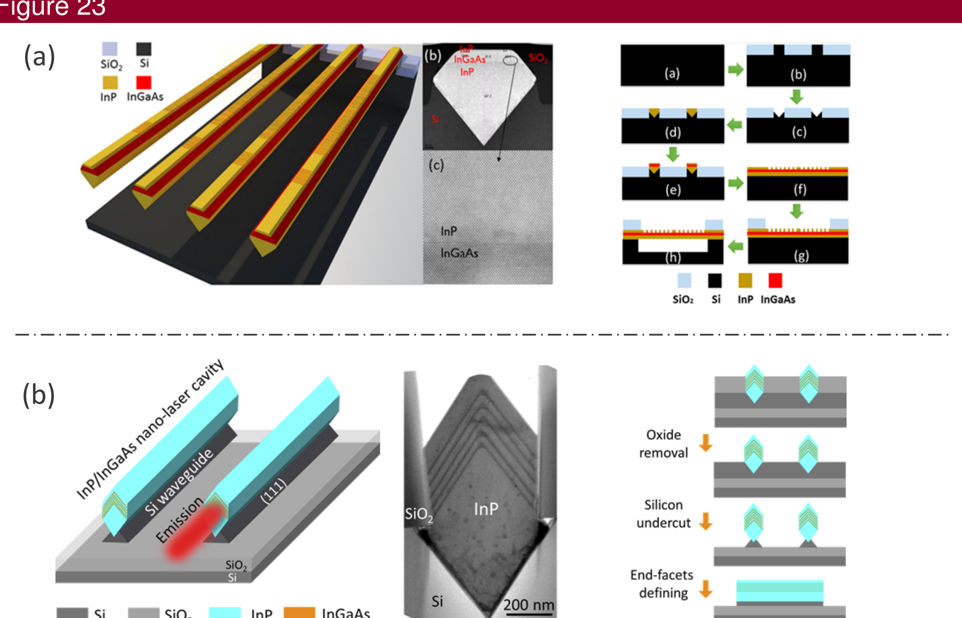

(a) InP DBF nano-ridge laser array grown on Si wafers with suspended cavities. Reprinted with permission from Tian *et al.*, Nano Lett. **17**, 559–564 (2017) [218]. Copyright 2017 American Chemical Society, https://doi.org/10.1021/ https://doi.org/10.1021/acs.nanolett.6b04690. (b) InP/InGaAs nano-ridge laser array selectively on SOI. Reprinted with permission from [219] © The Optical Society.

higher defect density whereas a narrower nano-ridge leads to poor light confinement and reduced optical gain. Second, as the refractive index between III–V and Si are quite similar, light cannot be tightly confined within the epitaxial nano-ridge and additional designs are required to achieve efficient waveguiding within the nano-ridge. As shown by the schematic in Fig. 23(a), researchers realized efficient waveguiding through selective removal of the Si layer underneath to form suspended InP nano-ridge structures [217,218]. They attained room-temperature single-mode lasing at 900 nm through patterning DFB gratings atop the smoothened InP nano-ridge. The authors later achieved lasing at the 1360 nm band by introducing an InGaAs QW inside the InP nano-ridge [218].

Another route to achieve tight light confinement within the III–V nano-ridge involves growing III–V nano-ridges on SOI wafers, which also allows for future light coupling with Si-waveguides (see Fig. 23(b)). Han *et al.* demonstrated the growth of III–V nano-ridges on (001) SOI wafers and adopted InGaAs/InP MQWs as active gain medium [220,221]. Tight mode confinement was obtained via selectively patterning the Si device layer. Room-temperature lasing at the 1550 nm band was reported from a 50-μm-long Fabry–Perot cavity and a 20-μm-long DBR laser as shown by the SEM images in Fig. 24(a) and the emission spectra in Fig. 24(b) [219,222]. The authors further designed a novel growth strategy to enable the growth of high-quality III–V nano-ridge inside trapezoidal troughs and then demonstrated the first telecom lasers directly grown on standard 220 nm SOI platforms for Si-photonics [223].

Compared with blanket heteroepitaxy, one advantage of selective heteroepitaxy is more efficient light coupling between the epitaxial III–V light sources and the Si waveguides. Calculated coupling efficient up to 97% can be obtained at the 1550 nm band between III–V nano-ridge and a Si rib waveguide [210]. However, one issue of light sources grown on Si by the ART method is associated with the inevitable

Figure 24

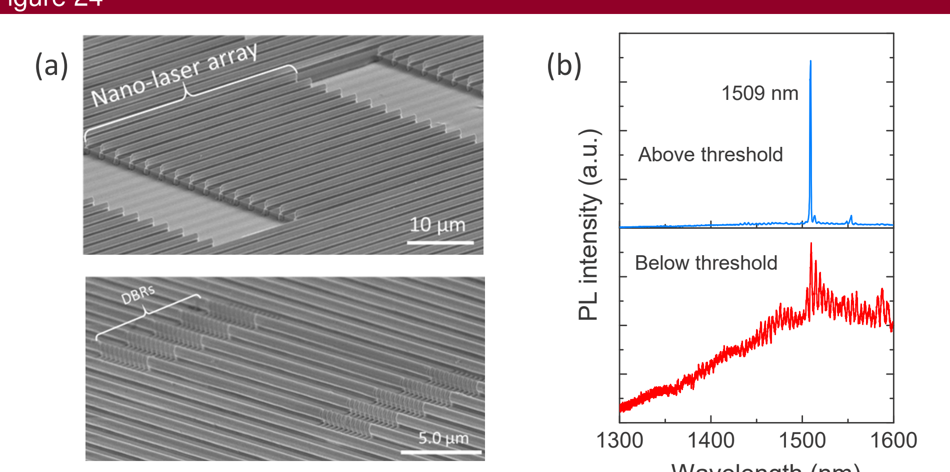

(a) SEM image of lasers with FP cavities selectively on SOI. (b) Emission spectra of the InP/InGaAs lasers at 1550 nm band. Reprinted with permission from [222] © The Optical Society.

overlap between the mode profile and the defective III–V/Si interface, which might cause absorption of the electromagnetic field by the dangling bonds and degrade the device performance. In terms of future electrically driven lasers, as the width of the nano-ridge is limited around a few hundred nanometers, the major challenge lies at how to pattern the metal pads on top of these sub-wavelength nano-ridges without introducing large optical propagation loss. Efforts targeted at this obstacle have started to emerge. Experimental demonstrations of PDs with a similar p–i–n structure have been reported using the ART approach and the influence of metal contacts on the optical absorption loss have also been studied theoretically [210,224].

5.1b. Nano-Ridge Engineering

The concept of nano-ridge engineering (NRE) involves manipulating the geometry of the epitaxial III–V crystal to the desired form via adjusting the growth parameters. As indicated by the schematic and SEM images in Fig. 25, the engineering of the nano-ridge is attained when the III–V nano-ridges grow out of the narrow oxide trench and enlarge into an air-cladded III–V waveguide [225]. The defect management of NRE is identical to that of the ART method and is completed within the narrow oxide trench. Both GaAs and GaSb nano-ridges have been successfully grown on (001) Si substrates using this NRE technique [208,226]. Compared with the ART approach, the NRE scheme could achieve III–V nano-ridges with a variety of geometries. In addition, it separates the guided optical modes from the defective III–V and oxide/Si interfaces.

The air-clad GaAs and GaSb nano-ridges outside the narrow oxide trench are excellent waveguides for wavelengths in the near-infrared range. As shown in Fig. 26(a), Shi *et al.* demonstrated GaAs/InGaAs nano-ridge lasers in the 1030 nm band through embedding multi-GaAs/InGaAs QWs inside the nano-ridge and passivating the GaAs nano-ridge using a thin InGaP cladding layer [216]. Single mode lasing is achieved via patterning DFB gratings on top of the nano-ridge structure. The authors later reported loss-coupled GaAs/InGaAs nano-ridge lasers emitting at the same wavelength range by replacing the etched GaAs gratings with patterned metallic gratings, as shown by the schematic in Fig. 26(b) [227]. This design might shed light on future realization of electrically driven devices as the metallic patterns could function as both mode

Figure 25

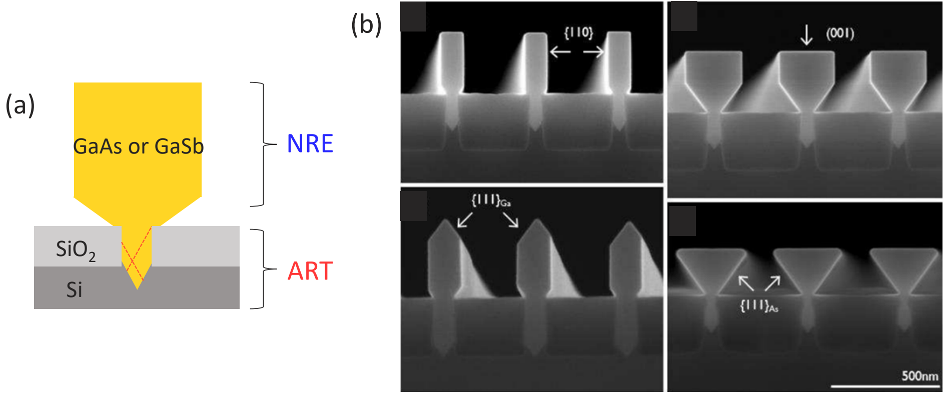

Basic concept of the nano-ridge engineering growth scheme. (a) Schematic and (b) SEM images GaAs nano-ridges with different geometries grow on (001) Si substrates. Reprinted with permission from Kunert *et al.*, ECS Trans. **75**, 409 (2016) [225], https://doi.org/10.1149/07508.0409ecst. © IOP Publishing. Reproduced with permission. All rights reserved.

Figure 26

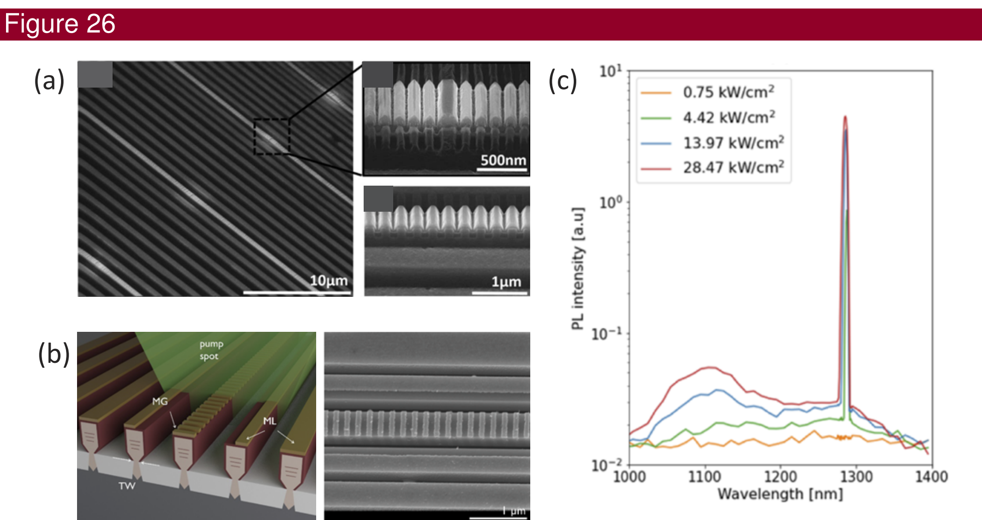

(a) Nano-ridge laser array with GaAs DFB gratings. Reprinted with permission from [216] © The Optical Society. (b) Nano-ridge laser array with metal gratings. Reprinted with permission from [228] © The Optical Society. (c) GaAs/InGaAs nano-ridge lasers emitting at 1030 nm and grown on (001) Si wafers. Reprinted with permission from [228] © The Optical Society.

selection gratings and carrier injection pads. Recently the authors reported lasing in the 1300 nm band through growing InGaAs nano-ridge structures and embedding QWs with higher indium compositions as displayed in Fig. 26(c) [228].

Similar to the ART method, the NRE method also realizes efficient light coupling between nano-ridge lasers and Si-waveguides using evanescent coupling strategies. As shown by the schematics in Fig. 27, three designs, namely directional coupler, linearly tapered coupler, and advanced adiabatic coupler, are evaluated and compared [229]. Simulated coupling efficiency up to 100% and a decoupling length of 200 µm is obtained for the advanced adiabatic coupler in the 1300 nm band. The NRE method has also enabled the demonstration of heterojunction bipolar transistors and waveguide

Figure 27

Light coupling schemes with Si-waveguides: directional coupler, linearly tapered coupler, and advanced adiabatic coupler. Reprinted with permission from [229] © The Optical Society.

Figure 28

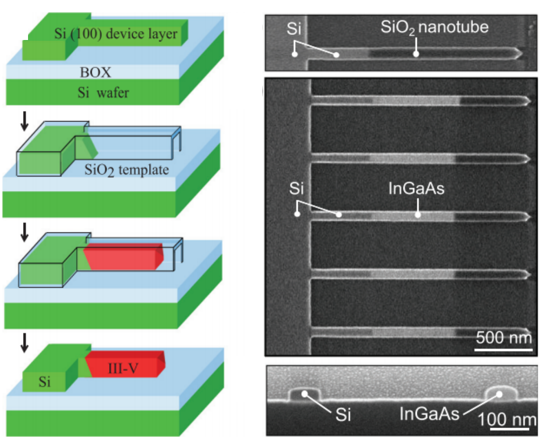

Basic concept of template-assisted selective epitaxy. Reprinted with permission from Schmid *et al.*, Appl. Phys. Lett. **106**, 233101 (2015) [233]. Copyright 2015, AIP Publishing LLC.

PDs using the GaAs nano-ridge as a basic building block [230,231]. The metal pads in the PDs were carefully designed to minimize the optical absorption loss, which can also be applied for future electrically driven lasers [231].

5.2. Lateral Integration Schemes

5.2a. Template-Assisted Selective Epitaxy

Template-assisted selective epitaxy (TASE) denotes the nucleation of III–V nanostructures from a tiny Si surface (generally sub-100 nm), and the evolution of the III–V crystal is guided by a hollow oxide template (Fig. 28) [232,233]. Nucleating III–V compounds from a sub-100 nm Si seed promotes the relaxation of misfit strain with elastic relaxation and consequently precludes the formation of TDs inside the epitaxial III–V material. In addition, initiating epitaxy from such a tiny seed allows for the growth of III–V compounds with a myriad of compositions including GaAs, InGaAs, InAs, GaSb, and InSb on Si substrate with different crystal phases such as (001)-oriented, (111)-oriented, and even poly-Si [233]. As the geometry of the epitaxial III–V crystal follows that of the hollow oxide template, the architecture of the III–V material grown on Si by TASE is highly versatile. Consequently, TASE has produced III–V crystals with a variety of geometries containing vertical/horizontal/stacked nanowires, micro-disks/rings, and photonic crystal cavities [232].

Figure 29

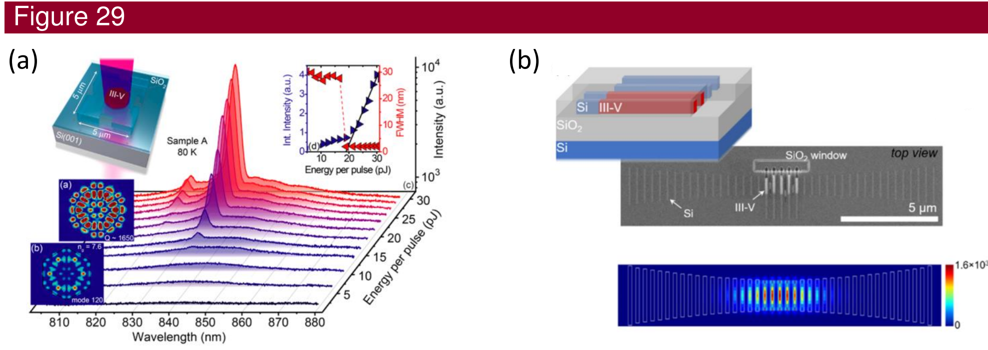

Micro-disk lasers

Photonic Crystal cavity

Lasers with different cavities grow on (001) Si by TASE. (a) and (b) refer to micro-disk cavities emitting at 850 nm and photonic crystal cavities emitting at telecom bands [234,237].Reprinted with permission from Wirths *et al.*, ACS Nano. **12**, 2169–2175 (2018) [234]. Copyright 2018 American Chemical Society, https://doi.org/10.1021/acsnano.7b07911. Reprinted with permission from Mauthe *et al.*, Nano Lett. **20**, 8768–8772 (2020) [237]. Copyright 2020 American Chemical Society, https://doi.org/10.1021/acs.nanolett.0c03634.

Similar to the ART approach, the TASE approach was first devised for the integration of high-performance III–V electron devices on Si [212] and later was introduced for the integration of III–V light sources on Si as the research of Si-photonics boomed in the last decade. As TASE produces III–V nano-structures with dimensions in the deep sub-wavelength scale, building light emitters from these crystals requires additional designs for tight mode confinement and sufficient material gain. One approach uses the hollow oxide template to alter the evolution of the GaAs nano-rod from the vertical direction to the horizontal direction and then transforms the GaAs nano-rod into a GaAs micro-disk (Fig. 29(a)) [234–236]. As the GaAs micro-disk is situated right on top of the oxide layer and is passivated with a thin layer of AlGaAs, the whispering-gallery mode can be supported and room-temperature lasing at the 850 nm band was thus achieved [234]. The other approach to build light sources from these tiny III–V nano-structures involves replacing the central Si nano-rods in a PhC with III–V nano-rods grown by the TASE method. As shown by the schematic, SEM image, and simulated mode profile in Fig. 29(b), the epitaxial III–V nano-rods overlaps with the maximum of the mode field profile and emission over the telecom band was subsequently obtained [232,237].

The intimate placement of the epitaxial III–V material with the Si device layer offered by the TASE approach also provides a nice platform for efficient light interfacing between the III–V light sources and the passive Si-waveguide. Figure 30 displays the design of a Si-waveguide coupled III–V p–i–n PD selectively grown on (001) SOI platform by the TASE approach [238,239]. Owing to the limited material volume of the epitaxial III–V, butt coupling was naturally adopted. The waveguided-coupled PD exhibits a responsivity up to 0.2 A/W at –2 V bias and a 3 dB bandwidth exceeding 70 G. Similar device design could be tailored for future electrically driven III–V nano-lasers selectively grown on SOI and intimately interfaced with the Si-based PICs.

5.2b. Lateral ART

The ART, NRE ,and TASE methods all produce high-quality, sub-wavelength III–V crystals on Si substrates. However, the realization of future electrically driven lasers necessitates larger-dimension III–V materials to minimize the metal-induced optical loss and to allow for more flexibility in device design [240–242]. As suggested by

Figure 30

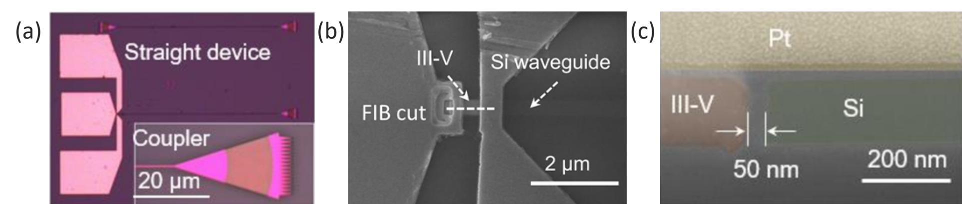

(a)–(c) Waveguide-coupled III–V PDs grown on (001) SOI wafers by TASE. Reprinted from [239] under a Creative Commons license.

Figure 31

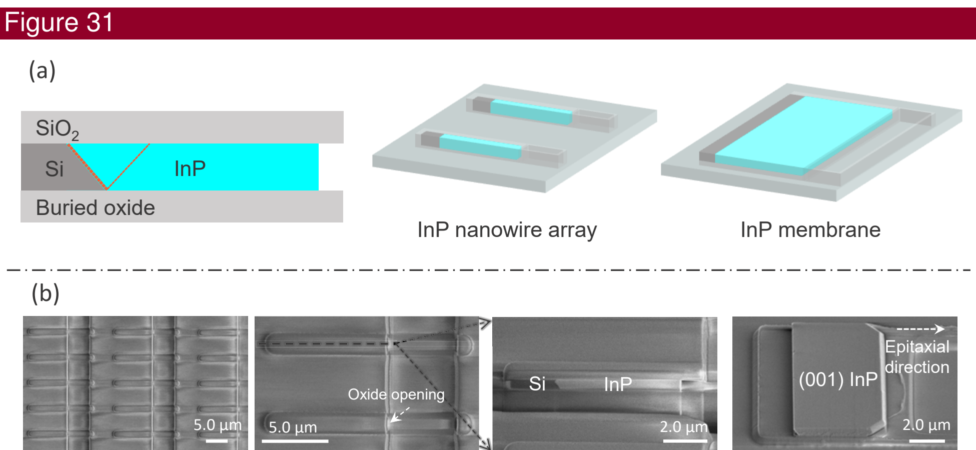

Concept of the lateral ART growth scheme. (a) Schematic showing the selective growth of InP nanowire array and large-dimension membranes on (001) SOI wafers. (b) SEM images of the InP crystals grown on SOI. Reprinted from [243] under a Creative Commons license.

the name, the lateral ART method shares an identical defect necking effect with the conventional vertical ART approach (Fig. 31(a)) [243,244]. Changing the growth direction from the vertical to the lateral unleashes a few unique advantages unavailable in the above selective growth strategies. First, the lateral ART method enables the growth of large-dimension III–V membrane on (001) SOI wafers. InP membrane with a width over 7.0 μm has been demonstrated recently [243–245]. In the vertical ART approach, growing wider nano-ridges compromises the defect necking effect. In sharp contrast, the defect necking effect of the lateral ART method hinges on the aspect ratio between the width of epitaxial III–V crystal and the thickness of the Si device layer. As a result, the defect necking effect is enhanced as the width of the III–V material enlarges. Second, the epitaxial III–V crystal features an in-plane configuration with the Si device layer as well as a unique characteristic of “III–V-on-insulator”. Third, when synergizing with the TASE method, the lateral ART approach allows for the growth of both III–V nanowire array and large-dimension membranes on SOI substrates as evidenced by the SEM images in Fig. 31(b). Such a monolithic InP-on-SOI platform offered by the lateral ART approach could enable the implementation of a variety of photonic functionalities that combines the respective advantages of both InP and Si.

Because the epitaxial III–V crystals by the lateral ART method are sandwiched by the top and bottom oxide layers, the resultant large index contrast leads to strong light confinement within the epitaxial III–V layer and, therefore, renders a unique platform for the design and fabrication of III–V lasers on SOI. Recently, Yan *et al.* demonstrated InP microwire laser array, InP square cavity laser array, and micro-disk lasers using

Figure 32

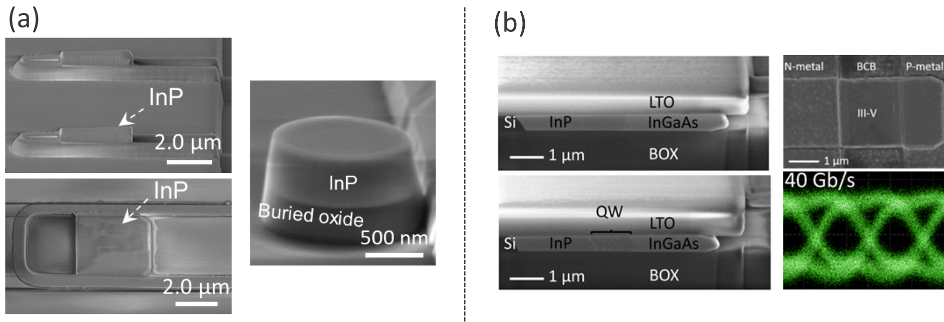

(a) Nanowire lasers, square cavity lasers, and micro-disk lasers on Si enabled by lateral ART. Reprinted from [243] under a Creative Commons license. (b) High-performance InP/InGaAs p–i–n PDs selectively grown on SOI by lateral ART [246]. Reprinted with permission from [246] © Copyright The Optical Society.

InP selectively grown on SOI by the lateral ART method [243]. Figure 32 (a) displays the SEM images of these three different types of laser. The microwire laser and square-cavity laser array were formed by the as-grown InP crystals after removing the adjacent Si device layer, whereas the micro-disk lasers were created by a series of top-down processing steps including photolithography and dry etching. As illustrated by the SEM images in Fig. 32(b), the laterally evolving InP can also be doped into p–i–n junctions and InGaAs active regions can be accordingly embedded. Most recently, Xue *et al.* demonstrated high-performance III–V PDs with a 3 dB bandwidth beyond 40 GHz and operating over the entire telecom band on this monolithic InP-on-SOI platform [246].

Compared with III–V nanostructures enabled by the other approaches, the large-dimension III–V membrane offered by the lateral ART method facilitates easier light coupling with Si-waveguides as well as the design of electrically driven lasers selectively grown on SOI. Both butt and evanescent coupling strategies have been proposed and simulated [210]. In addition, the large-dimension InP can be tailored by top-down processing into a variety of geometries, for instance tapers, to further improve the coupling efficiency with the Si-waveguide. Figures 33(a)–33(c) present the proposed electrically driven lasers with a lateral p–i–n structure selectively grown on SOI by the lateral ART method. In this scenario, the active gain medium is selectively regrown using the epitaxial InP as a substrate. Light can be tightly confined within the central ridge structure and metal-induced propagation loss is negligible when the width of the epitaxial InP exceeds 4.0 μm. The configuration of this design has been demonstrated using InP membranes bonded on to SOI wafers [247].

6. SUMMARY AND PERSPECTIVE

In this paper, we have reviewed recent advances in light sources integrated onto mainstream Si platform and discussed four different technologies: light sources built from Group IV semiconductors, heterogeneous integration of III–V light sources on Si, blanket heteroepitaxy of III–V light sources on Si, and selective heteroepitaxy of III–V light sources on Si. In the past few years, there have been tremendous progress in each technology, and these innovations bring us closer to a fully integrated, low-cost, and multi-functional Si-based PIC. In Group IV light sources, band engineering of Ge/Sn compounds transformed the otherwise indirect Group IV semiconductors into direct-band materials with higher light-emitting efficiency, and subsequently, both

Figure 33

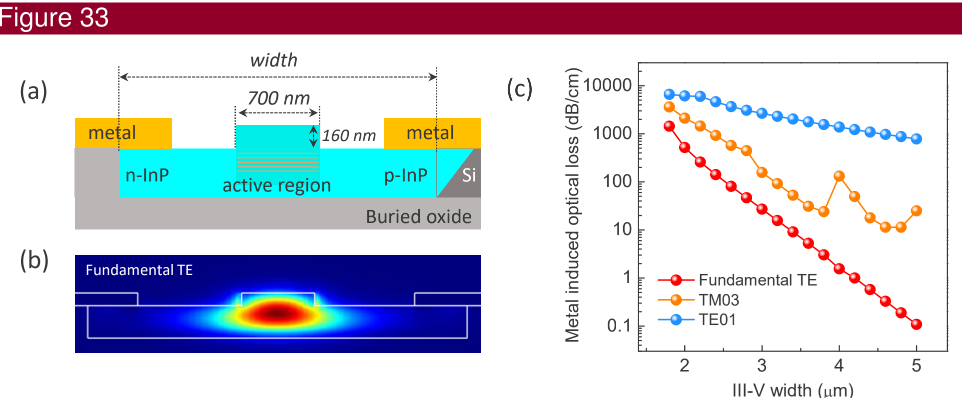

(a)–(c) Proposed device structure of electrically driven lasers based on the lateral ART scheme. © 2021 IEEE. Reprinted, with permission, from Han *et al.*, J. Lightw. Technol. **39**, 940–948 (2021) [210]. Copyright 2021 IEEE.

optically pumped and electrically pumped mid-infrared GeSn lasers have been demonstrated experimentally. Parallel to the investigation of Group IV lasers, the research of integrating III–V light emitters on Si are evolving rapidly. Novel technologies were developed and a few of them are now commercialized. The heterogeneous bonding approach continues to combine the optimized metrics of the active III–V and the passive Si and demonstrates devices with unprecedented performance; the best example is narrow-linewidth lasers integrated onto SiN platforms. Micro-transfer printing allows for the large-scale integration of pre-fabricated III–V light sources on Si and further improves the integration density of the heterogeneous integration approach. Meanwhile the monolithic integration of III–V lasers on Si via direct heteroepitaxy has thrived in the past few years and receives intensive investigation from both academia and industry. O-band QD laser didoes grown on GaAs/Si templates using blanket heteroepitaxy are now poised for commercial deployment as these devices manifest excellent reliability in high-temperature environment and the performance is on par with those grown on native GaAs substrates. Selective heteroepitaxy enables the growth of a complete suite of TD-free III–V compound semiconductors on predefined areas on Si wafers. More significantly, these epitaxial III–V lasers can be intimately positioned with the Si device layer and the light can be readily coupled into the Si waveguides. Analogous to selectively grown Ge-PDs available in Si-photonics foundries, selective area growth of III–V lasers on Si could potentially be the ultimate solution for future densely-integrated Si PICs and OEICs.

Despite these impressive advances, there remain several roadblocks and obstacles. Table 2 summarizes the major challenges and future research opportunities of each technology. Among them, heterogeneous integration via bonding is the only commercially viable approach as it delivers the best device performance and elegantly combines the best of both III–V compounds and Group IV semiconductors. However, neither bonding nor transfer printing is a monolithic integration approach. They are perfect candidates for applications in the short term, whereas monolithic solutions for densely integrated Si-PICs may be developed in the long run. In terms of monolithic integration approaches, light sources grown on Si must meet several critical requirements before being considered for commercial deployment. First, the light sources should operate under cw electrically pumping conditions. In this case, the paramount issue for Group IV lasers is to achieve direct bandgap of the GeSn compounds. For selective heteroepitaxy of III–V lasers on Si, the focus should be further increasing the dimension of the epitaxial III–V material to reduce the optical loss induced by

Table 2. Challenges and Opportunities of Each Technology

Technology	Challenges and Perspectives
Ge/Sn lasers on Si	a. Improve band structure for RT laser operation. b. Reduce TD density to enhance device reliability.
Heterogeneous integration of III–V lasers on Si	a. Improve thermal dissipation of III–V devices on SOI. b. Further reduce cost through recycling of III–V substrates.
Blanket heteroepitaxy of III–V lasers on Si	a. Realize efficient light coupling with Si-WGs. b. Reduce TD density for InP and GaSb grown on Si.
Selective heteroepitaxy of III–V lasers on Si	a. Realize electrically driven lasers. b. Extend the size of epitaxial III–V for flexible device implementation.

the metal contacts. Second, the devices should work reliably at high temperatures. In this regard, it is critical to achieve epitaxial active materials with low TD densities, especially for GeSn alloys grown on Si as well as InP and GaSb thin films grown on Si using blanket heteroepitaxy where the TD density is still of the order of 10^7–10^8 cm^{-2} [176,190]. Third, light from the lasers on Si must be efficiently coupled into Si-waveguides. This has been the most urgent issue in blanket heteroepitaxy of III–V lasers on Si as the thick buffer layer mandatory for defect reduction severely impedes the light interfacing with Si waveguides. Fourth, both the growth and fabrication of the light sources on Si should be compatible with the existing processes in standard Si photonics foundries. This feature requires the active gain material to be grown on (001)-oriented Si/SOI wafers with careful management of contamination and thermal budget.

DISCLOSURES

The authors declare no conflicts of interest.

DATA AVAILABILITY

No new data were generated or analyzed in the presented research.

REFERENCES

1. B. Jalali and S. Fathpour, “Silicon photonics,” J. Lightwave Technol. **24**, 4600–4615 (2006).
2. D. Thomson, A. Zilkie, J. E. Bowers, T. Komljenovic, G. T. Reed, L. Vivien, D. Marris-Morini, E. Cassan, L. Virot, J.-M. Fédéli, J.-M. Hartmann, J. H. Schmid, D.-X. Xu, F. Boeuf, P. O’Brien, G. Z. Mashanovich, and M. Nedeljkovic, “Roadmap on silicon photonics,” J. Opt. **18**, 073003 (2016).
3. R. Jones, P. Doussiere, J. B. Driscoll, W. Lin, H. Yu, Y. Akulova, T. Komljenovic, and J. E. Bowers, “Heterogeneously integrated InP/silicon photonics: fabricating fully functional transceivers,” IEEE Nanotechn. Mag. **13**(2), 17–26 (2019).
4. N. Margalit, C. Xiang, S. M. Bowers, A. Bjorlin, R. Blum, and J. E. Bowers, “Perspective on the future of silicon photonics and electronics,” Appl. Phys. Lett. **118**, 220501 (2021).
5. A. H. Atabaki, S. Moazeni, F. Pavanello, H. Gevorgyan, J. Notaros, L. Alloatti, M. T. Wade, C. Sun, S. A. Kruger, H. Meng, K. Al Qubaisi, I. Wang, B. Zhang, A. Khilo, C. V. Baiocco, M. Popovi, V. M. Stojanovi, and R. J. Ram, “Integrating photonics with silicon nanoelectronics for the next generation of systems on a chip,” Nature **556**, 349–354 (2018).
6. R. Soref, D. Buca, and S.-Q. Yu, “Group IV photonics: driving integrated optoelectronics,” Opt. Photon. News **27**(1), 32–39 (2016).

7. G. T. Reed, G. Mashanovich, F. Yand Gardes, and D. J. Thomson, "Silicon optical modulators," Nat. Photonics **4**, 518–526 (2010).
8. J. Michel, J. Liu, and L. C. Kimerling, "High-performance Ge-on-Si photodetectors," Nat. Photonics **4**, 527–534 (2010).
9. A. W. Elshaari, W. Pernice, K. Srinivasan, O. Benson, and V. Zwiller, "Hybrid integrated quantum photonic circuits," Nat. Photonics **14**, 285–298 (2020).
10. D. A. Miller, "Attojoule optoelectronics for low-energy information processing and communications," J. Lightwave Technol. **35**, 346–396 (2017).
11. C. Doerr and L. Chen, "Silicon photonics in optical coherent systems," Proc. IEEE **106**, 2291–2301 (2018).
12. D. Liang, A. Roshan-Zamir, Y.-H. Fan, C. Zhang, B. Wang, A. Descos, W. Shen, K. Yu, C. Li, G. Fan, G. Kurczveil, Y. Hu, Z. Huang, M. Fiorentino, S. Kumar, S. M. Palermo, and R.-G. Beausoleil, "Fully-integrated heterogeneous DML transmitters for high-performance computing," J. Lightwave Technol. **38**, 3322–3337 (2020).
13. T. Hu, B. Dong, X. Luo, T.-Y. Liow, J. Song, C. Lee, and G.-Q. Lo, "Silicon photonic platforms for mid-infrared applications," Photonics Res. **5**, 417–430 (2017).
14. H. Lin, Z. Luo, T. Gu, L. C. Kimerling, K. Wada, A. Agarwal, and J. Hu, "Mid-infrared integrated photonics on silicon: a perspective," Nanophotonics **7**, 393–420 (2017).
15. D. Marpaung, C. Roeloffzen, R. Heideman, A. Leinse, S. Sales, and J. Capmany, "Integrated microwave photonics," Laser Photonics Rev. **7**, 506–538 (2013).
16. D. Liang and J. E. Bowers, "Recent progress in lasers on silicon," Nat. Photonics **4**, 511–517 (2010).
17. Y. Urino, T. Usuki, J. Fujikata, M. Ishizaka, K. Yamada, T. Horikawa, T. Nakamura, and Y. Arakawa, "High-density optical interconnects by using silicon photonics," Proc. SPIE **9010**, 901006 (2014).
18. T. Shimizu, N. Hatori, M. Okano, M. Ishizaka, Y. Urino, T. Yamamoto, M. Mori, T. Nakamura, and Y. Arakawa, "High density hybrid integrated light source with a laser diode array on a silicon optical waveguide platform for inter-chip optical interconnection," in *8th IEEE International Conference on Group IV Photonics*, pp. 181–183. IEEE, 2011.
19. Z. Fang, Q. Y. Chen, and C. Z. Zhao, "A review of recent progress in lasers on silicon," Opt. Laser Technol. **46**, 103–110 (2013).
20. Z. Zhou, B. Yin, and J. Michel, "On-chip light sources for silicon photonics," Light: Sci. Appl. **4**, e358 (2015).
21. C. Cornet, Y. Léger, and C. Robert, *Integrated Lasers on Silicon*. Elsevier, 2016.
22. Z. Wang, A. Abbasi, and U. Dave, *et al.*, "Novel light source integration approaches for silicon photonics," Laser Photonics Rev. **11**, 1700063 (2017).
23. M. Buffolo, C. De Santi, J. Norman, C. Shang, J. E. Bowers, G. Meneghesso, E. Zanoni, and M. Meneghini, "A review of the reliability of integrated IR laser diodes for silicon photonics," Electronics **10**, 2734 (2021).
24. S. Wirths, D. Buca, and S. Mantl, "Si–Ge–Sn alloys: from growth to applications," Prog. Cryst. Growth Charact. Mater. **62**, 1–39 (2016).
25. T. Komljenovic, M. Davenport, J. Hulme, A. Y. Liu, C. T. Santis, A. Spott, S. Srinivasan, E. J. Stanton, C. Zhang, and J. E. Bowers, "Heterogeneous silicon photonic integrated circuits," J. Lightwave Technol. **34**, 20–35 (2016).
26. J. Zhang, G. Muliuk, and J. Juvert, *et al.*, "III–V-on-Si photonic integrated circuits realized using micro-transfer-printing," APL Photonics **4**, 110803 (2019).
27. T. Wang, H. Liu, A. Lee, F. Pozzi, and A. Seeds, "1.3-μm InAs/GaAs quantum-dot lasers monolithically grown on Si substrates," Opt. Express **19**, 11381–11386 (2011).

28. A. Y. Liu, S. Srinivasan, J. Norman, A. C. Gossard, and J. E. Bowers, “Quantum dot lasers for silicon photonics,” Photonics Res. **3**, B1–B9 (2015).
29. Y. Han and K. M. Lau, “III–V lasers selectively grown on (001) silicon,” J. Appl. Phys. **128**, 200901 (2020).
30. M. Smit, K. Williams, and J. van der Tol, “Past, present, and future of InP-based photonic integration,” APL Photonics **4**, 050901 (2019).
31. R. Geiger, T. Zabel, and H. Sigg, “Group IV direct band gap photonics: methods, challenges, and opportunities,” Front. Mater. **2**, 52 (2015).
32. K. Dohnalová and K. Kůsová, “Optical properties of Si nanocrystals enhanced by ligands,” in *Silicon Photonics IV*, pp. 3–65. Springer, Cham, 2021.
33. A. J. Kenyon, “Erbium in silicon,” Semicond. Sci. Technol. **20**, R65–R84 (2005).
34. H. Rong, A. Liu, R. Jones, O. Cohen, D. Hak, R. Nicolaescu, A. Fang, and M. Paniccia, “An all-silicon Raman laser,” Nature **433**, 292–294 (2005).
35. J. Liu, X. Sun, D. Pan, X. Wang, L. C. Kimerling, T. L. Koch, and J. Michel, “Tensile-strained, n-type Ge as a gain medium for monolithic laser integration on Si,” Opt. Express **15**, 11272–11277 (2007).
36. S. Wirths, R. Geiger, N. Von Den Driesch, G. Mussler, T. Stoica, S. Mantl, Z. Ikonic, M. Luysberg, S. Chiussi, J. M. Hartmann, H. Sigg, J. Faist, D. Buca, and D. Grützmacher, “Lasing in direct-bandgap GeSn alloy grown on Si,” Nat. Photonics **9**, 88–92 (2015).
37. Y. Zhou, Y. Miao, S. Ojo, H. Tran, G. Abernathy, J. M. Grant, S. Amoah, G. Salamo, W. Du, J. Liu, J. Margetis, J. Tolle, Y.-h. Zhang, G. Sun, R. A. Soref, B. Li, and S.-Q. Yu, “Electrically injected GeSn lasers on Si operating up to 100 K,” Optica **7**, 924–928 (2020).
38. V. Reboud, D. Buca, H. Sigg, J. M. Hartmann, Z. Ikonic, N. Pauc, V. Calvo, P. Rodriguez, and A. Chelnokov, “Lasing in Group-IV materials,” Silicon Photon. IV **139**, 105–195 (2021).
39. M. A. Green, J. Zhao, A. Wang, P. J. Reece, and M. Gal, “Efficient silicon light-emitting diodes,” Nature **412**(6849), 805–808 (2001).
40. W. L. Ng, M. A. Lourenco, R. M. Gwilliam, S. Ledain, G. Shao, and K. P. Homewood, “An efficient room-temperature silicon-based light-emitting diode,” Nature **410**, 192–194 (2001).
41. L. T. Canham, “Silicon quantum wire array fabrication by electrochemical and chemical dissolution of wafers,” Appl. Phys. Lett. **57**, 1046–1048 (1990).
42. B. Gelloz and N. Koshida, “Electroluminescence with high and stable quantum efficiency and low threshold voltage from anodically oxidized thin porous silicon diode,” J. Appl. Phys. **88**, 4319–4324 (2000).
43. M. H. Nayfeh, S. Rao, N. Barry, J. Therrien, G. Belomoin, A. Smith, and S. Chaieb, “Observation of laser oscillation in aggregates of ultrasmall silicon nanoparticles,” Appl. Phys. Lett. **80**, 121–123 (2002).
44. N. Koshida and H. Koyama, “Visible electroluminescence from porous silicon,” Appl. Phys. Lett. **60**, 347–349 (1992).
45. L. Pavesi, L. Dal Negro, C. Mazzoleni, G. Franzo, and D. F. Priolo, “Optical gain in silicon nanocrystals,” Nature **408**, 440–444 (2000).
46. G. Franzò, S. Boninelli, D. Pacifici, F. Priolo, F. Iacona, and C. Bongiorno, “Sensitizing properties of amorphous Si clusters on the 1.54-μm luminescence of Er in Si-rich SiO_2,” Appl. Phys. Lett. **82**, 3871–3873 (2003).
47. L. Yang, D. K. Armani, and K. J. Vahala, “Fiber-coupled erbium microlasers on a chip,” Appl. Phys. Lett. **83**, 825–826 (2003).
48. A. Polman, B. Min, J. Kalkman, T. J. Kippenberg, and K. J. Vahala, “Ultralow-threshold erbium-implanted toroidal microlaser on silicon,” Appl. Phys. Lett. **84**, 1037–1039 (2004).

49. M. A. Ferrara and L. Sirleto, "Integrated Raman laser: a review of the last two decades," Micromachines **11**, 330 (2020).
50. H. Rong, R. Jones, A. Liu, O. Cohen, D. Hak, A. Fang, and M. Paniccia, "A continuous-wave Raman silicon laser," Nature **433**, 725–728 (2005).
51. H. Rong, S. Xu, Y.-H. Kuo, V. Sih, O. Cohen, O. Raday, and M. Paniccia, "Low-threshold continuous-wave Raman silicon laser," Nat. Photonics **1**, 232–237 (2007).
52. Y. Zhang, K. Zhong, and H. K. Tsang, "Raman lasing in multimode silicon racetrack resonators," Laser Photonics Rev. **15**, 2000336 (2021).
53. M. Ahmadi, W. Shi, and S. LaRochelle, "Widely tunable silicon Raman laser," Optica **8**, 804–810 (2021).
54. V. Reboud, A. Gassenq, J. M. Hartmann, J. Widiez, L. Virot, J. Aubin, K. Guilloy, S. Tardif, J. M. Fédéli, N. Pauc, A. Chelnokov, and V. Calvo, "Germanium based photonic components toward a full silicon/germanium photonic platform," Prog. Cryst. Growth Charact. Mater. **63**, 1–24 (2017).
55. M. J. Süess, R. Geiger, R. A. Minamisawa, G. Schiefler, J. Frigerio, D. Chrastina, G. Isella, R. Spolenak, J. Faist, and H. Sigg, "Analysis of enhanced light emission from highly strained germanium microbridges," Nat. Photonics **7**, 466–472 (2013).
56. F. T. Armand Pilon, A. Lyasota, Y.-M. Niquet, V. Reboud, V. Calvo, N. Pauc, J. Widiez, C. Bonzon, J. M. Hartmann, A. Chelnokov, J. Faist, and H. Sigg, "Lasing in strained germanium microbridges," Nat. Commun. **10**, 1–8 (2019).
57. C. Boztug, J. R. Sánchez-Pérez, F. F. Sudradjat, R. B. Jacobson, D. M. Paskiewicz, M. G. Lagally, and R. Paiella, "Tensilely strained germanium nanomembranes as infrared optical gain media," Small **9**, 622–630 (2013).
58. A. Elbaz, M. El Kurdi, A. Aassime, S. Sauvage, X. Checoury, I. Sagnes, C. Baudot, F. Boeuf, and P. Boucaud, "Germanium microlasers on metallic pedestals," APL Photonics **3**, 106102 (2018).
59. J. Liu, X. Sun, R. Camacho-Aguilera, L. C. Kimerling, and J. Michel, "Ge-on-Si laser operating at room temperature," Opt. Lett. **35**, 679–681 (2010).
60. R. E. Camacho-Aguilera, Y. Cai, N. Patel, J. T. Bessette, M. Romagnoli, L. C. Kimerling, and J. Michel, "An electrically pumped germanium laser," Opt. Express **20**, 11316–11320 (2012).
61. L. Carroll, P. Friedli, S. Neuenschwander, H. Sigg, S. Cecchi, F. Isa, D. Chrastina, G. Isella, Y. Fedoryshyn, and J. Faist, "Direct-gap gain and optical absorption in germanium correlated to the density of photoexcited carriers, doping, and strain," Phys. Rev. Lett. **109**, 057402 (2012).
62. M. S. Vitiello, G. Scalari, B. Williams, and P. De Natale, "Quantum cascade lasers: 20 years of challenges," Opt. Express **23**, 5167–5182 (2015).
63. G. Dehlinger, L. Diehl, U. Gennser, H. Sigg, J. Faist, K. Ensslin, D. Grützmacher, and E. Müller, "Intersubband electroluminescence from silicon-based quantum cascade structures," Science **290**, 2277–2280 (2000).
64. D. J. Paul, "The progress towards terahertz quantum cascade lasers on silicon substrates," Laser Photonics Rev. **4**, 610–632 (2010).
65. L. Spindlberger, J. Aberl, A. Polimeni, J. Schuster, J. Hörschläger, T. Truglas, H. Groiss, F. Schäffler, T. Fromherz, and M. Brehm, "In-situ annealing and hydrogen irradiation of defect-enhanced germanium quantum dot light sources on silicon," Crystals **10**, 351 (2020).
66. E. M. Fadaly, A. Dijkstra, J. R. Suckert, D. Ziss, M. A. J. van Tilburg, C. Mao, Y. Ren, V. T. van Lange, K. Korzun, S. Kölling, M. A. Verheijen, D. Busse, C. Rödl, J. Furthmüller, F. Bechstedt, J. Stangl, J. J. Finley, S. Botti, J. E. M. Haverkort, and E. P. A. M. Bakkers, "Direct-bandgap emission from hexagonal Ge and SiGe alloys," Nature **580**, 205–209 (2020).

67. K. P. Homewood and M. A. Lourenço, "The rise of the GeSn laser," Nat. Photonics **9**, 78–79 (2015).
68. V. Reboud, A. Gassenq, N. Pauc, J. Aubin, L. Milord, Q. M. Thai, M. Bertrand, K. Guilloy, D. Rouchon, J. Rothman, T. Zabel, F. Armond Pilon, H. Sigg, A. Chelnokov, J. M. Hartmann, and V. Calvo, "Optically pumped GeSn micro-disks with 16% Sn lasing at 3.1 μ m up to 180 K," Appl. Phys. Lett. **111**, 092101 (2017).
69. Y. Zhou, W. Dou, W. Du, S. Ojo, H. Tran, S. A. Ghetmiri, J. Liu, G. Sun, R. Soref, J. Margetis, J. Tolle, B. Li, Z. Chen, M. Mortazavi, and S.-Q. Yu, "Optically pumped GeSn lasers operating at 270 K with broad waveguide structures on Si," ACS Photonics **6**, 1434–1441 (2019).
70. J. Chrétien, N. Pauc, F. A. Pilon, M. Bertrand, Q.-M. Thai, L. Casiez, N. Bernier, H. Dansas, P. Gergaud, E. Delmadeleine, R. Khazaka, H. Sigg, J. Faist, A. Chelnokov, V. Reboud, J.-M. Hartmann, and V. Calvo, "GeSn lasers covering a wide wavelength range thanks to uniaxial tensile strain," ACS Photonics **6**, 2462–2469 (2019).
71. B. Wang, E. Sakat, E. Herth, M. Gromovyi, A. Bjelajac, J. Chaste, G. Patriarche, P. Boucaud, F. Boeuf, N. Pauc, V. Calvo, J. Chrétien, M. Frauenrath, A. Chelnokov, V. Reboud, J.-M. Hartmann, and M. El Kurdi, "GeSnOI mid-infrared laser technology," Light: Sci. Appl. **10**, 1–13 (2021).
72. A. Elbaz, D. Buca, N. von den Driesch, K. Pantzas, G. Patriarche, N. Zerounian, E. Herth, X. Checoury, S. Sauvage, I. Sagnes, A. Foti, R. Ossikovski, J.-M. Hartmann, F. Boeuf, Z. Ikonic, P. Boucaud, D. Grützmacher, and M. El Kurdi, "Ultra-low-threshold continuous-wave and pulsed lasing in tensile-strained GeSn alloys," Nat. Photonics **14**, 375–382 (2020).
73. D. Stange, N. von den Driesch, T. Zabel, F. Armand-Pilon, D. Rainko, B. Marzban, P. Zaumseil, J. -M. Hartmann, Z. Ikonic, G. Capellini, S. Mantl, H. Sigg, J. Witzens, D. Grtzmacher, and D. Buca, "GeSn/SiGeSn heterostructure and multi quantum well lasers," ACS Photonics **5**, 4628–4636 (2018).
74. S. Ojo, "Si-based electrically injected GeSn lasers," in SPIE Photonics West, Vol. 15, p. 11995 (SPIE, 2020).
75. S. Lindgren, H. Ahlfeldt, L. Backlin, L. Forssen, C. Vieider, H. Elderstig, M. Svensson, L. Granlund, L. Andersson, B. Kerzar, B. Broberg, O. Kjebon, R. Schatz, E. Forzelius, and S. Nilsson, "24-GHz modulation bandwidth and passive alignment of flip-chip mounted DFB laser diodes," IEEE Photonics Technol. Lett. **9**, 306–308 (1997).
76. G. Roelkens, D. L. Liu Liu, R. Jones, A. Fang, B. Koch, and J. Bowers, "III-V/silicon photonics for on-chip and intra-chip optical interconnects," Laser Photonics Rev. **4**, 751–779 (2010).
77. J. M. Ramirez, H. Elfaiki, T. Verolet, C. Besancon, A. Gallet, D. Nel, K. Hassan, S. Olivier, C. Jany, S. Malhouitre, K. Gradkowski, P.E. Morrissey, P. O'Brien, C. Caillaud, N. Vaissire, J. Decobert, S. Lei, R. Enright, A. Shen, and M. Achouche, "III–V-on-silicon integration: from hybrid devices to heterogeneous photonic integrated circuits," IEEE J. Sel. Top. Quantum Electron. **26**, 1–13 (2020).
78. G. Roelkens, J. Van Campenhout, J. Brouckaert, D. Van Thourhout, R. Baets, P. Rojo Romeo, P. Regreny, A. Kazmierczak, C. Seassal, X. Letartre, G. Hollinger, J. M. Fedeli, L. Di Cioccio, and C. Lagahe-Blanchard, "III–V/Si photonics by die-to-wafer bonding," Mater. Today **10**(7-8), 36–43 (2007).
79. X. Guo, A. He, and Y. Su, "Recent advances of heterogeneously integrated III–V laser on Si," J. Semicond. **40**, 101304 (2019).
80. O. Marshall, M. Hsu, Z. Wang, B. Kunert, C. Koos, and D. Van Thourhout, "Heterogeneous integration on silicon photonics," Proc. IEEE **106**, 2258–2269 (2018).

81. J. Yoon, S. Lee, D. Kang, M. A. Meitl, C. A. Bower, and J. A. Rogers, "Heterogeneously integrated optoelectronic devices enabled by micro-transfer printing," Adv. Opt. Mater. **3**, 1313–1335 (2015).
82. C. Xiang, W. Jin, D. Huang, M. A. Tran, J. Guo, Y. Wan, W. Xie, G. Kurczveil, A. M. Netherton, D. Liang, H. Rong, and J. E. Bowers, "High-performance silicon photonics using heterogeneous integration," IEEE J. Sel. Top. Quantum Electron. **28**, 1–15 (2022).
83. D. Liang, A. W. Fang, H. Park, T. E. Reynolds, K. Warner, D. C. Oakley, and J. E. Bowers, "Low-temperature, strong SiO2-SiO2 covalent wafer bonding for III–V compound semiconductors-to-silicon photonic integrated circuits," J. Electron. Mater. **37**, 1552–1559 (2008).
84. S. Keyvaninia, M. Muneeb, S. Stankovi, P. J. Van Veldhoven, D. Van Thourhout, and G. Roelkens, "Ultra-thin DVS-BCB adhesive bonding of III–V wafers, dies and multiple dies to a patterned silicon-on-insulator substrate," Opt. Mater. Express **3**, 35–46 (2013).
85. R. H. Esser, K. D. Hobart, and F. J. Kub, "Improved low-temperature Si-Si hydrophilic wafer bonding," J. Electrochem. Soc. **150**, G228–G231 (2003).
86. T. Hong, G.-Z. Ran, T. Chen, J.-Q. Pan, W.-X. Chen, Y. Wang, Y.-B. Cheng, S. Liang, L.-J. Zhao, L.-Q. Yin, J.-H. Zhang, W. Wang, and G.-G. Qin, "A selective-area metal bonding InGaAsP–Si laser," IEEE Photonics Technol. Lett. **22**, 1141–1143 (2010).
87. T. Hong, Y.-P. Li, W.-X. Chen, G.-Z. Ran, G.-G. Qin, H.-L. Zhu, S. Liang, Y. Wang, J.-Q. Pan, and W. Wang, "Bonding InGaAsP/ITO/Si hybrid laser with ITO as cathode and light-coupling material," IEEE Photonics Technol. Lett. **24**, 712–714 (2012).
88. K. Tanabe, K. Watanabe, and Y. Arakawa, "III–V/Si hybrid photonic devices by direct fusion bonding," Sci. Rep. **2**, 349 (2012).
89. F. Niklaus, P. Enoksson, E. Kälvesten, and G. Stemme, "Low-temperature full wafer adhesive bonding," J. Micromech. Microeng. **11**, 100–107 (2001).
90. A. W. Fang, H. Park, O. Cohen, R. Jones, M. J. Paniccia, and J. E. Bowers, "Electrically pumped hybrid AlGaInAs-silicon evanescent laser," Opt. Express **14**, 9203–9210 (2006).
91. H. Park, Y.-h. Kuo, A. W. Fang, R. Jones, O. Cohen, M. J. Paniccia, and J. E. Bowers, "A hybrid AlGaInAs-silicon evanescent preamplifier and photodetector," Opt. Express **15**, 13539–13546 (2007).
92. J. Van Campenhout, P. Rojo-Romeo, D. Van Thourhout, C. Seassal, P. Regreny, L. Di Cioccio, J.-M. Fedeli, and R. Baets, "Thermal characterization of electrically injected thin-film InGaAsP microdisk lasers on Si," J. Lightwave Technol. **25**, 1543–1548 (2007).
93. A. W. Fang, E. Lively, D. L. Ying-Hao Kuo, and J. E. Bowers, "A distributed feedback silicon evanescent laser," Opt. Express **16**, 4413–4419 (2008).
94. A. W. Fang, B. R. Koch, R. Jones, E. Lively, D. Liang, Y.-H. Kuo, and J. E. Bowers, "A distributed Bragg reflector silicon evanescent laser," IEEE Photonics Technol. Lett. **20**, 1667–1669 (2008).
95. X. Sun, A. Zadok, M. J. Shearn, K. A. Diest, A. Ghaffari, H. A. Atwater, A. Scherer, and A. Yariv, "Electrically pumped hybrid evanescent Si/InGaAsP lasers," Opt. Lett. **34**, 1345–1347 (2009).
96. D. Liang, M. Fiorentino, T. Okumura, H.-H. Chang, D. T. Spencer, Y.-H. Kuo, A. W. Fang, D. Dai, R. G. Beausoleil, and J. E. Bowers, "Electrically-pumped compact hybrid silicon microring lasers for optical interconnects," Opt. Express **17**, 20355–20364 (2009).
97. A. Alduino, L. Liao, and R. Jones, *et al.*, "Demonstration of a high speed 4-channel integrated silicon photonics WDM link with hybrid silicon lasers," in

Integrated Photonics Research, Silicon and Nanophotonics and Photonics in Switching, OSA Technical Digest (CD) (Optical Society of America, 2010), paper PDIWI5.

98. G. Kurczveil, M. J. Heck, J. D. Peters, J. M. Garcia, D. Spencer, and J. E. Bowers, "An integrated hybrid silicon multiwavelength AWG laser," IEEE J. Sel. Top. Quantum Electron. **17**, 1521–1527 (2011).
99. H. Park, M. N. Sysak, H.-W. Chen, A. W. Fang, D. Liang, L. Liao, B. R. Koch, J. Bovington, Y. Tang, K. Wong, M. Jacob-Mitos, R. Jones, and J. E. Bowers, "Device and integration technology for silicon photonic transmitters," IEEE J. Sel. Top. Quantum Electron. **17**, 671–688 (2011).
100. X. Zheng, S. Lin, Y. Luo, J. Yao, G. Li, S. S. Djordjevic, J.-H. Lee, H. D. Thacker, I. Shubin, K. Raj, J. E. Cunningham, and A. V. Krishnamoorthy, "Efficient WDM laser sources towards terabyte/s silicon photonic interconnects," J. Lightwave Technol. **31**, 4142–4154 (2013).
101. B. R. Koch, E. J. Norberg, B. Kim, J. Hutchinson, J. Shin, G. Fish, and A. Fang, "Integrated silicon photonic laser sources for telecom and datacom," in *Optical Fiber Communication Conference/National Fiber Optic Engineers Conference 2013*, OSA Technical Digest (online) (Optical Society of America, 2013), paper PDP5C.8.
102. K. Takeda, T. Sato, T. Fujii, E. Kuramochi, M. Notomi, K. Hasebe, T. Kakitsuka, and S. Matsuo, "Heterogeneously integrated photonic-crystal lasers on silicon for on/off chip optical interconnects," Opt. Express **23**, 702–708 (2015).
103. G. Crosnier, D. Sanchez, S. Bouchoule, P. Monnier, G. Beaudoin, I. Sagnes, R. Raj, and F. Raineri, "Hybrid indium phosphide-on-silicon nanolaser diode," Nat. Photonics **11**, 297–300 (2017).
104. Z. Wang, K. Van Gasse, V. Moskalenko, S. Latkowski, E. Bente, B. Kuyken, and G. Roelkens, "A III–V-on-Si ultra-dense comb laser," Light: Sci. Appl. **6**, e16260 (2017).
105. R. Wang, S. Sprengel, A. Malik, A. Vasiliev, G. Boehm, R. Baets, M.-C. Amann, and G. Roelkens, "Heterogeneously integrated III–V-on-silicon 2.3µm distributed feedback lasers based on a type-II active region," Appl. Phys. Lett. **109**, 221111 (2016).
106. D. Shin, J. Cha, S. Kim, Y. Shin, K. Cho, K. Ha, G. Jeong, H. Hong, K. Lee, and H.-K. Kang, "O-band DFB laser heterogeneously integrated on a bulk-silicon platform," Opt. Express **26**, 14768–14774 (2018).
107. M. L. Davenport, S. Liu, and J. E. Bowers, "Integrated heterogeneous silicon/III–V mode-locked lasers," Photonics Res. **6**, 468–478 (2018).
108. H. Park, C. Zhang, M. A. Tran, and T. Komljenovic, "Heterogeneous silicon nitride photonics," Optica **7**, 336–337 (2020).
109. B. Li, W. Jin, L. Wu, L. Chang, H. Wang, B. Shen, Z. Yuan, A. Feshali, M. Paniccia, K. Vahala, and J. E. Bowers, "Reaching fiber-laser coherence in integrated photonics," Opt. Lett. **46**, 5201–5204 (2021).
110. S. Keyvaninia, G. Roelkens, D. Van Thourhout, C. Jany, M. Lamponi, A. Le Liepvre, F. Lelarge, D. Make, G.-H. Duan, D. Bordel, and J.-M. Fedeli, "Demonstration of a heterogeneously integrated III–V/SOI single wavelength tunable laser," Opt. Express **21**, 3784–3792 (2013).
111. T. Komljenovic, S. Srinivasan, E. Norberg, M. Davenport, G. Fish, and J. E. Bowers, "Widely tunable narrow-linewidth monolithically integrated external-cavity semiconductor lasers," IEEE J. Sel. Top. Quantum Electron. **21**, 214–222 (2015).
112. S. Dhoore, G. Roelkens, and G. Morthier, "III–V-on-silicon three-section DBR laser with over 12 nm continuous tuning range," Opt. Lett. **42**, 1121–1124 (2017).

113. D. Huang, M. A. Tran, J. Guo, J. Peters, T. Komljenovic, A. Malik, P. A. Morton, and J. E. Bowers, "High-power sub-kHz linewidth lasers fully integrated on silicon," Optica **6**, 745–752 (2019).
114. M. A. Tran, D. Huang, J. Guo, T. Komljenovic, P. A. Morton, and J. E. Bowers, "Ring-resonator based widely-tunable narrow-linewidth Si/InP integrated lasers," IEEE J. Sel. Top. Quantum Electron. **26**, 1–14 (2020).
115. M. A. Tran, D. Huang, and J. E. Bowers, "Tutorial on narrow linewidth tunable semiconductor lasers using Si/III–V heterogeneous integration," APL Photonics **4**, 111101 (2019).
116. J. F. Bauters, "Planar waveguides with less than 0.1 dB/m propagation loss fabricated with wafer bonding," Opt. Express **19**, 24090–24101 (2011).
117. T. J. Morin, L. Chang, W. Jin, C. Li, J. Guo, H. Park, M. A. Tran, T. Komljenovic, and J. E. Bowers, "CMOS-foundry-based blue and violet photonics," Optica **8**, 755–756 (2021).
118. C. Xiang, J. Liu, J. Guo, L. Chang, R. N. Wang, W. Weng, J. Peters, W. Xie, Z. Zhang, J. Riemensberger, J. Selvidge, T. J. Kippenberg, and J. E. Bowers, "Laser soliton microcombs heterogeneously integrated on silicon," Science **373**, 99–103 (2021).
119. G. Roelkens, J. Zhang, A. De Groote, J. Juvert, N. Ye, S. Kumari, J. Goyvaerts, G. Muliuk, S. Uvin, G. Chen, B. Haq, B. Snyder, J. Van Campenhout, D. Van Thourhout, A. J. Trindade, C. A. Bower, J. O'Callaghan, R. Loi, B. Roycroft, and B. Corbett, "Transfer printing for silicon photonics transceivers and interposers," in *2018 IEEE Optical Interconnects Conference (OI)* (IEEE, USA, 2018), pp. 13–14.
120. M. A. Meitl, Z.-T. Zhu, V. Kumar, K. J. Lee, X. Feng, Y. Y. Huang, I. Adesida, R. G. Nuzzo, and J. A. Rogers, "Transfer printing by kinetic control of adhesion to an elastomeric stamp," Nat. Mater. **5**, 33–38 (2006).
121. J. Justice, C. Bower, M. Meitl, M. B. Mooney, M. A. Gubbins, and B. Corbett, "Wafer-scale integration of group III–V lasers on silicon using transfer printing of epitaxial layers," Nat. Photonics **6**, 610–614 (2012).
122. H. Yang, D. Zhao, S. Chuwongin, J.-H. Seo, W. Yang, Y. Shuai, J. Berggren, M. Hammar, Z. Ma, and W. Zhou, "Transfer-printed stacked nanomembrane lasers on silicon," Nat. Photonics **6**, 615–620 (2012).
123. J. Zhang, C. O. de Beeck, B. Haq, B. Kuyken, D. Van Thourhout, J. Van Campenhout, G. Lepage, P. Verheyen, A. Gocalinska, S. Cuyvers, E. Pelucchi, B. Corbett, A. Hermans, A. J. Trindade, C. Bower, R. Baets, G. Roelkens, and G. Morthier, "III–V-on-Si/SiN lasers realized using micro-transfer-printing," Proc. SPIE **11705**, 16 (2021).
124. B. Corbett, R. Loi, J. O'Callaghan, and G. Roelkens, "Transfer printing for silicon photonics," in *Semiconductors and Semimetals*, vol. 99, pp. 43–70. Elsevier, 2018.
125. A. De Groote, P. Cardile, A. Z. Subramanian, A. M. Fecioru, C. Bower, D. Delbeke, R. Baets, and G. Roelkens, "Transfer-printing-based integration of single-mode waveguide-coupled III–V-on-silicon broadband light emitters," Opt. Express **24**, 13754–13762 (2016).
126. J. Goyvaerts, S. Kumari, S. Uvin, J. Zhang, R. Baets, A. Gocalinska, E. Pelucchi, B. Corbett, and G. Roelkens, "Transfer-print integration of GaAs pin photodiodes onto silicon nitride waveguides for near-infrared applications," Opt. Express **28**, 21275–21285 (2020).
127. B. Haq, S. Kumari, K. Van Gasse, J. Zhang, A. Gocalinska, E. Pelucchi, B. Corbett, and G. Roelkens, "Micro-transfer-printed III-V-on-silicon C-band semiconductor optical amplifiers," Laser Photon. Rev. **14**, 1900364 (2020).

128. J. Juvert, T. Cassese, S. Uvin, A. De Groote, B. Snyder, L. Bogaerts, G. Jamieson, J. Van Campenhout, G. Roelkens, and D. Van Thourhout, "Integration of etched facet, electrically pumped, C-band Fabry-Pérot lasers on a silicon photonic integrated circuit by transfer printing," Opt. Express **26**, 21443–21454 (2018).
129. B. Haq, J. R. Vaskasi, J. Zhang, A. Gocalinska, E. Pelucchi, B. Corbett, and G. Roelkens, "Micro-transfer-printed III–V-on-silicon C-band distributed feedback lasers," Opt. Express **28**, 32793–32801 (2020).
130. J. Zhang, Y. Li, S. Dhoore, G. Morthier, and G. Roelkens, "Unidirectional, widely-tunable and narrow-linewidth heterogeneously integrated III–V-on-silicon laser," Opt. Express **25**, 7092–7100 (2017).
131. C. O. de Beeck, B. Haq, L. Elsinger, A. Gocalinska, E. Pelucchi, B. Corbett, G. Roelkens, and B. Kuyken, "Heterogeneous III–V on silicon nitride amplifiers and lasers via microtransfer printing," Optica **7**, 386–393 (2020).
132. S. Cuyvers, B. Haq, C. O. de Beeck, S. Poelman, A. Hermans, Z. Wang, A. Gocalinska, E. Pelucchi, B. Corbett, G. Roelkens, K. Van Gasse, and B. Kuyken, "Low noise heterogeneous III-V-on-silicon-nitride mode-locked comb laser," Laser Photonics Rev. **15**, 2000485 (2021).
133. J. Goyvaerts, A. Grabowski, J. Gustavsson, S. Kumari, A. Stassen, R. Baets, A. Larsson, and G. Roelkens, "Enabling VCSEL-on-silicon nitride photonic integrated circuits with micro-transfer-printing," Optica **8**, 1573–1580 (2021).
134. S. F. Fang, K. Adomi, S. Iyer, H. Morkoc, H. Zabel, C. Choi, and N. Otsuka, "Gallium arsenide and other compound semiconductors on silicon," J. Appl. Phys. **68**, R31–R58 (1990).
135. Y. B. Bolkhovityanov and O. P. Pchelyakov, "GaAs epitaxy on Si substrates: modern status of research and engineering," Phys.-Usp. **51**, 437–456 (2008).
136. Q. Li and K. M. Lau, "Epitaxial growth of highly mismatched III–V materials on (001) silicon for electronics and optoelectronics," Prog. Cryst. Growth Charact. Mater. **63**, 105–120 (2017).
137. M. Akiyama, Y. Kawarada, and K. Kaminishi, "Growth of GaAs on Si by MOVCD," J. Cryst. Growth **68**, 21–26 (1984).
138. R. Fischer, H. Morkoc, D. A. Neumann, H. Zabel, C. Choi, N. Otsuka, M. Longerbone, and L. P. Erickson, "Material properties of high-quality GaAs epitaxial layers grown on Si substrates," J. Appl. Phys. **60**, 1640–1647 (1986).
139. M. Bou Sanayeh, A. Jaeger, W. Schmid, S. Tautz, P. Brick, K. Streubel, and G. Bacher, "Investigation of dark line defects induced by catastrophic optical damage in broad-area AlGaInP laser diodes," Appl. Phys. Lett. **89**, 101111 (2006).
140. S. Chen, W. Li, J. Wu, Q. Jiang, M. Tang, S. Shutts, S. N. Elliott, A. Sobiesierski, A.J. Seeds, I. Ross, P. M. Smowton, and H. Liu, "Electrically pumped continuous-wave III–V quantum dot lasers on silicon," Nat. Photonics **10**, 307–311 (2016).
141. M. Martin, D. Caliste, R. Cipro, R. Alcotte, J. Moeyaert, S. David, F. Bassani, T. Cerba, Y. Bogumilowicz, E. Sanchez, Z. Ye, X. Y. Bao, J. B. Pin, T. Baron, and P. Pochet, "Toward the III–V/Si co-integration by controlling the biatomic steps on hydrogenated Si (001)," Appl. Phys. Lett. **109**, 253103 (2016).
142. K. Li, J. Yang, and Y. Lu, *et al.*, "Inversion boundary annihilation in GaAs monolithically grown on on-axis silicon (001)," Adv. Opt. Mater. **8**, 2000970 (2020).
143. K. Volz, A. Beyer, W. Witte, J. Ohlmann, I. Németh, B. Kunert, and W. Stolz, "GaP-nucleation on exact Si (001) substrates for III/V device integration," J. Cryst. Growth **315**, 37–47 (2011).
144. Q. Li, K. W. Ng, and K. M. Lau, "Growing antiphase-domain-free GaAs thin films out of highly ordered planar nanowire arrays on exact (001) silicon," Appl. Phys. Lett. **106**, 072105 (2015).

145. Y. Wan, Q. Li, A. Y. Liu, W. W. Chow, A. C. Gossard, J. E. Bowers, E. L. Hu, and K. M. Lau, "Sub-wavelength InAs quantum dot micro-disk lasers epitaxially grown on exact Si (001) substrates," Appl. Phys. Lett. **108**, 221101 (2016).
146. M. Paladugu, C. Merckling, R. Loo, O. Richard, H. Bender, J. Dekoster, W. Vandervorst, M. Caymax, and M. Heyns, "Site selective integration of III–V materials on Si for nanoscale logic and photonic devices," Cryst. Growth Des. **12**, 4696–4702 (2012).
147. J. C. Norman, Daehwan Jung, A. Y. Liu, Jennifer Selvidge, Kunal Mukherjee, J. E. Bowers, and R. W. Herrick, "Reliability of lasers on silicon substrates for silicon photonics," in *Reliability of Semiconductor Lasers and Optoelectronic Devices*, pp. 239–271. Woodhead Publishing, 2021.
148. D. Jung, R. Herrick, J. Norman, K. Turnlund, C. Jan, K. Feng, A. C. Gossard, and J. E. Bowers, "Impact of threading dislocation density on the lifetime of InAs quantum dot lasers on Si," Appl. Phys. Lett. **112**, 153507 (2018).
149. C. Shang, E. Hughes, Y. Wan, M. Dumont, R. Koscica, J. Selvidge, R. Herrick, A. C. Gossard, K. Mukherjee, and J. E. Bowers, "High-temperature reliable quantum-dot lasers on Si with misfit and threading dislocation filters," Optica **8**, 749–754 (2021).
150. D. Bimberg, N. Kirstaedter, N. N. Ledentsov, Z. I. Alferov, P. S. Kop'Ev, and V. M. Ustinov, "InGaAs-GaAs quantum-dot lasers," IEEE J. Sel. Top. Quantum Electron. **3**, 196–205 (1997).
151. A. Y. Liu, C. Zhang, J. Norman, A. Snyder, D. Lubyshev, J. M. Fastenau, A. W. Liu, A. C. Gossard, and J. E. Bowers, "High performance continuous wave 1.3 μm quantum dot lasers on silicon," Appl. Phys. Lett. **104**, 041104 (2014).
152. Y. Wan, J. Norman, Q. Li, M. J. Kennedy, D. Liang, C. Zhang, D. Huang, Z. Zhang, A. Y. Liu, A. Torres, D. Jung, A. C. Gossard, E. L. Hu, K. M. Lau, and J. E. Bowers, "1.3 μm submilliamp threshold quantum dot micro-lasers on Si," Optica **4**, 940–944 (2017).
153. Y. Wan, S. Zhang, J. C. Norman, M. J. Kennedy, W. He, S. Liu, C. Xiang, C. Shang, J.-J. He, A. C. Gossard, and J. E. Bowers, "Tunable quantum dot lasers grown directly on silicon," Optica **6**, 1394–1400 (2019).
154. J.-M. Oh, C. C. Venters, C. Di, A. M. Pinto, L. Wan, I. Younis, Z. Cai, C. Arai, B. R. So, J. Duan, and G. Dreyfuss, "Continuous-wave quantum dot photonic crystal lasers grown on on-axis Si (001)," Nat. Commun. **11**, 1–7 (2020).
155. T. Zhou, M. Tang, H. Li, Z. Zhang, Y. Cui, J.-S. Park, M. Martin, T. Baron, S. Chen, H. Liu, and Z. Zhang, "Single-mode photonic crystal nanobeam lasers monolithically grown on Si for dense integration," IEEE J. Sel. Top. Quantum Electron. **28**, 1–6 (2022).
156. Y. Wang, S. Chen, Y. Yu, L. Zhou, L. Liu, C. Yang, M. Liao, M. Tang, Z. Liu, J. Wu, W. Li, I. Ross, A. J. Seeds, H. Liu, and S. Yu, "Monolithic quantum-dot distributed feedback laser array on silicon," Optica **5**, 528–533 (2018).
157. J. Kwoen, B. Jang, J. Lee, T. Kageyama, K. Watanabe, and Y. Arakawa, "All MBE grown InAs/GaAs quantum dot lasers on on-axis Si (001)," Opt. Express **26**, 11568–11576 (2018).
158. Z.-H. Wang, W.-Q. Wei, Q. Feng, T. Wang, and J.-J. Zhang, "InAs/GaAs quantum dot single-section mode-locked lasers on Si (001) with optical self-injection feedback," Opt. Express **29**, 674–683 (2021).
159. S. Liu, X. Wu, D. Jung, J. C. Norman, M. J. Kennedy, H. K. Tsang, A. C. Gossard, and J. E. Bowers, "High-channel-count 20 GHz passively mode-locked quantum dot laser directly grown on Si with 4.1 Tbit/s transmission capacity," Optica **6**, 128–134 (2019).
160. J. C. Norman, D. Jung, Y. Wan, and J. E. Bowers, "Perspective: the future of quantum dot photonic integrated circuits," APL Photonics **3**, 030901 (2018).

161. M. Tang, J.-S. Park, Z. Wang, S. Chen, P. Jurczak, A. Seeds, and H. Liu, "Integration of III–V lasers on Si for Si photonics," Prog. Quantum Electron. **66**, 1–18 (2019).
162. B. Shi, Y. Han, Q. Li, and K. M. Lau, "1.55-μm lasers epitaxially grown on silicon," IEEE J. Sel. Top. Quantum Electron. **25**, 1–11 (2019).
163. S. Liu and A. Khope, "Latest advances in high-performance light sources and optical amplifiers on silicon," J. Semicond. **42**, 041307 (2021).
164. W. Yang, Y. Li, F. Meng, H. Yu, M. Wang, P. Wang, G. Luo, X. Zhou, and J. Pan, "III–V compound materials and lasers on silicon," J. Semicond. **40**, 101305 (2019).
165. A. Y. Liu and J. Bowers, "Photonic integration with epitaxial III–V on silicon," IEEE J. Sel. Top. Quantum Electron. **24**, 1–12 (2018).
166. S. Pan, V. Cao, M. Liao, Y. Lu, Z. Liu, M. Tang, S. Chen, A. Seeds, and H. Liu, "Recent progress in epitaxial growth of III–V quantum-dot lasers on silicon substrate," J. Semicond. **40**, 101302 (2019).
167. S. Shutts, P. M. Smowton, and A. B. Krysa, "Dual-wavelength InP quantum dot lasers," Appl. Phys. Lett. **104**, 241106 (2014).
168. W. Luo, L. Lin, J. Huang, Y. Han, and K. M. Lau, "Red-emitting InP quantum dot micro-disk lasers epitaxially grown on (001) silicon," Opt. Lett. **46**, 4514–4517 (2021).
169. P. Dhingra, P. Su, B. D. Li, R. D. Hool, A. J. Muhowski, M. Kim, D. Wasserman, J. Dallesasse, and M. L. Lee, "Low-threshold InP quantum dot and InGaP quantum well visible lasers on silicon (001)," Optica **8**, 1495–1500 (2021).
170. B. Shi and J. Klamkin, "Defect engineering for high quality InP epitaxially grown on on-axis (001) Si," J. Appl. Phys. **127**, 033102 (2020).
171. L. Megalini, S. Tommaso, Š. Brunelli, W. O. Charles, A. Taylor, B. Isaac, J. E. Bowers, and J. Klamkin, "Strain-compensated InGaAsP superlattices for defect reduction of InP grown on exact-oriented (001) patterned Si substrates by metal organic chemical vapor deposition," Materials **11**, 337 (2018).
172. B. Shi, S. Zhu, Q. Li, Y. Wan, E. L. Hu, and K. M. Lau, "Continuous-wave optically pumped 1.55 μm InAs/InAlGaAs quantum dot microdisk lasers epitaxially grown on silicon," ACS Photonics **4**, 204–210 (2017).
173. B. Shi, Q. Li, Y. Wan, K. W. Ng, X. Zou, C. W. Tang, and K. M. Lau, "InAlGaAs/InAlAs MQWs on Si substrate," IEEE Photonics Technol. Lett. **27**, 748–751 (2015).
174. T. Sasaki, H. Mori, M. Tachikawa, and T. Yamada, "Aging tests of InP-based laser diodes heteroepitaxially grown on Si substrates," J. Appl. Phys. **84**, 6725–6728 (1998).
175. D. D. Nolte, "Surface recombination, free-carrier saturation, and dangling bonds in InP and GaAs," Solid-State Electron. **33**, 295–298 (1990).
176. B. Shi, H. Zhao, L. Wang, B. Song, S. Tommaso, S. Brunelli, and J. Klamkin, "Continuous-wave electrically pumped 1550 nm lasers epitaxially grown on on-axis (001) silicon," Optica **6**, 1507–1514 (2019).
177. L. Lin, Y. Xue, J. Li, W. Luo, J. Huang, and K. M. Lau, "C and L band room-temperature continuous-wave InP-based microdisk lasers grown on silicon," Opt. Lett. **46**, 2836–2839 (2021).
178. Y. Xue, W. Luo, S. Zhu, L. Lin, B. Shi, and K. M. Lau, "1.55 μm electrically pumped continuous wave lasing of quantum dash lasers grown on silicon," Opt. Express **28**, 18172–18179 (2020).
179. B. Shi, S. Zhu, Q. Li, C. W. Tang, Y. Wan, E. L. Hu, and K. M. Lau, "1.55 μm room-temperature lasing from subwavelength quantum-dot microdisks directly grown on (001) Si," Appl. Phys. Lett. **110**(12), 121109 (2017).

180. S. Zhu, B. Shi, Q. Li, and K. M. Lau, “1.5 μm quantum-dot diode lasers directly grown on CMOS-standard (001) silicon,” Appl. Phys. Lett. **113**, 221103 (2018).
181. B. Shi, S. Pinna, H. Zhao, S. Zhu, and J. Klamkin, “Lasing characteristics and reliability of 1550 nm laser diodes monolithically grown on silicon,” Phys. Status Solidi A **218**, 2000374 (2021).
182. R. Balasubramanian, V. Sichkovskyi, C. Corley-Wiciak, F. Schnabel, L. Popilevsky, G. Atiya, I. Khanonkin, A. J. Willinger, O. Eyal, G. Eisenstein, and J. P. Reithmaier, “High optical gain in InP-based quantum-dot material monolithically grown on silicon emitting at telecom wavelengths,” Semicond. Sci. Technol. **37**, 055005 (2022).
183. E. Tournié and L. Cerutti, *Mid-Infrared Optoelectronics*, 1st ed. (Elsevier, 2020).
184. K. Akahane, N. Yamamoto, S.-I. Gozu, and N. Ohtani, “Heteroepitaxial growth of GaSb on Si (001) substrates,” J. Cryst. Growth **264**, 21–25 (2004).
185. Y. H. Kim, J. Lee, Y. G. Noh, M. D. Kim, S. M. Cho, Y. J. Kwon, and J. E. Oh, “Growth mode and structural characterization of GaSb on Si (001) substrate: a transmission electron microscopy study,” Appl. Phys. Lett. **88**, 241907 (2006).
186. Z. Yan, Y. Han, and K. M. Lau, “InAs nano-ridges and thin films grown on (001) silicon substrates,” J. Appl. Phys. **128**, 035302 (2020).
187. Q. Li, B. Lai, and K. M. Lau, “Epitaxial growth of GaSb on V-grooved Si (001) substrates with an ultrathin GaAs stress relaxing layer,” Appl. Phys. Lett. **111**, 172103 (2017).
188. C. A. Wang, “Progress and continuing challenges in GaSb-based III–V alloys and heterostructures grown by organometallic vapor-phase epitaxy,” J. Cryst. Growth **272**, 664–681 (2004).
189. W. Zhou, W. Tang, and K. M. Lau, “A strain relief mode at interface of GaSb/GaAs grown by metalorganic chemical vapor deposition,” Appl. Phys. Lett. **99**, 221917 (2011).
190. M. Rio Calvo, L. Monge Bartolomé, M. Bahriz, G. Boissier, L. Cerutti, J.-B. Rodriguez, and E. Tournié, “Mid-infrared laser diodes epitaxially grown on on-axis (001) silicon,” Optica **7**, 263 (2020).
191. J.-R. Reboul, L. Cerutti, J.-B. Rodriguez, P. Grech, and E. Tournié, “Continuous-wave operation above room temperature of GaSb-based laser diodes grown on Si,” Appl. Phys. Lett. **99**, 121113 (2011).
192. J. Tatebayashi, A. Jallipalli, M. N. Kutty, S. Huang, K. Nunna, G. Balakrishnan, L. Ralph Dawson, and D. L. Huffaker, “Monolithically integrated III-Sb-based laser diodes grown on miscut Si substrates,” IEEE J. Sel. Top. Quantum Electron. **15**, 716–723 (2009).
193. L. Monge-Bartolome, B. Shi, B. Lai, G. Boissier, L. Cerutti, J.-B. Rodriguez, K. M. Lau, and E. Tournié, “GaSb-based laser diodes grown on MOCVD GaAs-on-Si templates,” Opt. Express **29**, 11268–11276 (2021).
194. H. Nguyen-Van, A. N. Baranov, Z. Loghmari, L. Cerutti, J.-B. Rodriguez, J. Tournet, G. Narcy, G. Boissier, G. Patriarche, M. Bahriz, E. Tourni, and R. Teissier, “Quantum cascade lasers grown on silicon,” Sci. Rep. **8**, 7206–7208 (2018).
195. L. Cerutti, D. A. Díaz Thomas, J.-B. Rodriguez, M. R. Calvo, G. Patriarche, A. N. Baranov, and E. Tournié, “Quantum well interband semiconductor lasers highly tolerant to dislocations,” Optica **8**, 1397–1402 (2021).
196. D. Chatzitheocharis, D. Ketzaki, C. Calò, C. Caillaud, and K. Vyrsokinos, “Design of Si-rich nitride interposer waveguides for efficient light coupling from InP-based QD-emitters to Si_3N_4 waveguides on a silicon substrate,” Opt. Express **28**, 34219–34236 (2020).

197. Y. Zhang, Y. Su, Y. Bi, J. Pan, H. Yu, Y. Zhang, J. Sun, X. Sun, and M. Chong, "Inclined emitting slotted single-mode laser with 1.7° vertical divergence angle for PIC applications," Opt. Lett. **43**, 86–89 (2018).
198. B. Kunert, Y. Mols, M. Baryshniskova, N. Waldron, A. Schulze, and R. Langer, "How to control defect formation in monolithic III/V hetero-epitaxy on (100) Si? A critical review on current approaches," Semicond. Sci. Technol. **33**, 093002 (2018).
199. J. Z. Li, J. Bai, J.-S. Park, B. Adekore, K. Fox, M. Carroll, A. Lochtefeld, and Z. Shellenbarger, "Defect reduction of GaAs epitaxy on Si (001) using selective aspect ratio trapping," Appl. Phys. Lett. **91**, 021114 (2007).
200. R. Cipro, T. Baron, M. Martin, J. Moeyaert, S. David, V. Gorbenko, F. Bassani, Y. Bogumilowicz, J. P. Barnes, N. Rochat, V. Loup, C. Vizioz, N. Allouti, N. Chauvin, X. Y. Bao, Z. Ye, J. B. Pin, and E. Sanchez, "Low defect InGaAs quantum well selectively grown by metal organic chemical vapor deposition on Si (100) 300 mm wafers for next generation non planar devices," Appl. Phys. Lett. **104**, 262103 (2014).
201. C. Merckling, N. Waldron, S. Jiang, W. Guo, N. Collaert, M. Caymax, E. Vancoille, K. Barla, A. Thean, M. Heyns, and W. Vandervorst, "Heteroepitaxy of InP on Si (001) by selective-area metal organic vapor-phase epitaxy in sub-50 nm width trenches: the role of the nucleation layer and the recess engineering," J. Appl. Phys. **115**, 023710 (2014).
202. Q. Li, Y. Han, X. Lu, and K. M. Lau, "GaAs-InGaAs-GaAs fin-array tunnel diodes on (001) Si substrates with room-temperature peak-to-valley current ratio of 5.4," IEEE Electron Device Lett. **37**, 24–27 (2016).
203. T. Orzali, A. Vert, B. O'Brian, J. L. Herman, S. Vivekanand, S. S. Papa Rao, and S. R. Oktyabrsky, "Epitaxial growth of GaSb and InAs fins on 300 mm Si (001) by aspect ratio trapping," J. Appl. Phys. **120**, 085308 (2016).
204. Y. Han, Q. Li, S.-P. Chang, W.-D. Hsu, and K. M. Lau, "Growing InGaAs quasi-quantum wires inside semi-rhombic shaped planar InP nanowires on exact (001) silicon," Appl. Phys. Lett. **108**, 242105 (2016).
205. S. Li, X. Zhou, M. Li, X. Kong, J. Mi, M. Wang, W. Wang, and J. Pan, "Ridge InGaAs/InP multi-quantum-well selective growth in nanoscale trenches on Si (001) substrate," Appl. Phys. Lett. **108**, 021902 (2016).
206. Y. Han, Q. Li, and K. M. Lau, "Highly ordered horizontal indium gallium arsenide/indium phosphide multi-quantum-well in wire structure on (001) silicon substrates," J. Appl. Phys. **120**, 245701 (2016).
207. L. Megalini, B. Bonef, B. C. Cabinian, H. Zhao, A. Taylor, J. S. Speck, J. E. Bowers, and J. Klamkin, "1550-nm InGaAsP multi-quantum-well structures selectively grown on v-groove-patterned SOI substrates," Appl. Phys. Lett. **111**, 032105 (2017).
208. B. Kunert, W. Guo, Y. Mols, B. Tian, Z. Wang, Y. Shi, D. Van Thourhout, M. Pantouvaki, J. Van Campenhout, R. Langer, and K. Barla, "III/V nano ridge structures for optical applications on patterned 300 mm silicon substrate," Appl. Phys. Lett. **109**, 091101 (2016).
209. P. Staudinger, S. Mauthe, N. V. Triviño, S. Reidt, K. E. Moselund, and H. Schmid, "Wurtzite InP microdisks: from epitaxy to room-temperature lasing," Nanotechnology **32**, 075605 (2021).
210. Y. Han, Y. Xue, Z. Yan, and K. M. Lau, "Selectively grown III–V lasers for integrated Si-photonics," J. Lightwave Technol. **39**, 940–948 (2021).
211. Y. Han, Q. Li, K. W. Ng, S. Zhu, and K. M. Lau, "InGaAs/InP quantum wires grown on silicon with adjustable emission wavelength at telecom bands," Nanotechnology **29**, 225601 (2018).

212. K. E. Moselund, H. Schmid, C. Bessire, M. T. Bjork, H. Ghoneim, and H. Riel, "InAs–Si nanowire heterojunction tunnel FETs," IEEE Electron Device Lett. **33**, 1453–1455 (2012).
213. N. Waldron, C. Merckling, L. Teugels, P. Ong, S. Ansar, U. Ibrahim, F. Sebaai, A. Pourghaderi, K. Barla, N. Collaert, and A. V.-Y. Thean, "InGaAs gate-all-around nanowire devices on 300mm Si substrates," IEEE Electron Device Lett. **35**, 1097–1099 (2014).
214. Y. Han, Q. Li, and K. M. Lau, "Fin-array tunneling trigger with tunable hysteresis on (001) silicon substrate," IEEE Electron Device Lett. **38**, 556–559 (2017).
215. Y. Han, Q. Li, and K. M. Lau, "Tristate memory cells using double-peaked fin-array III–V tunnel diodes monolithically grown on (001) silicon substrates," IEEE Trans. Electron Devices **64**, 4078–4083 (2017).
216. Y. Shi, Z. Wang, J. Van Campenhout, M. Pantouvaki, W. Guo, B. Kunert, and D. Van Thourhout, "Optical pumped InGaAs/GaAs nano-ridge laser epitaxially grown on a standard 300-mm Si wafer," Optica **4**, 1468–1473 (2017).
217. Z. Wang, B. Tian, M. Pantouvaki, W. Guo, P. Absil, J. Van Campenhout, C. Merckling, and D. Van Thourhout, "Room-temperature InP distributed feedback laser array directly grown on silicon," Nat. Photonics **9**, 837–842 (2015).
218. B. Tian, Z. Wang, M. Pantouvaki, P. Absil, J. Van Campenhout, C. Merckling, and D. Van Thourhout, "Room temperature O-band DFB laser array directly grown on (001) silicon," Nano Lett. **17**, 559–564 (2017).
219. Y. Han, W. K. Ng, Y. Xue, Q. Li, K. S. Wong, and K. M. Lau, "Telecom InP/InGaAs nanolaser array directly grown on (001) silicon-on-insulator," Opt. Lett. **44**, 767–770 (2019).
220. Y. Han, Q. Li, S. Zhu, K. W. Ng, and K. M. Lau, "Continuous-wave lasing from InP/InGaAs nanoridges at telecommunication wavelengths," Appl. Phys. Lett. **111**, 212101 (2017).
221. Y. Han, W. K. Ng, C. Ma, Q. Li, S. Zhu, C. C. S. Chan, K. W. Ng, S. Lennon, R. A. Taylor, K. S. Wong, and K. M. Lau, "Room-temperature InP/InGaAs nano-ridge lasers grown on Si and emitting at telecom bands," Optica **5**, 918–923 (2018).
222. Y. Han, W. K. Ng, Y. Xue, K. S. Wong, and K. M. Lau, "Room temperature III–V nanolasers with distributed Bragg reflectors epitaxially grown on (001) silicon-on-insulators," Photonics Res. **7**, 1081–1086 (2019).
223. Y. Han, Z. Yan, W. K. Ng, Y. Xue, K. S. Wong, and K. M. Lau, "Bufferless 1.5 µm III–V lasers grown on Si-photonics 220 nm silicon-on-insulator platforms," Optica **7**, 148–153 (2020).
224. Y. Xue, Y. Han, Y. Wang, Z. Zhang, H. K. Tsang, and K. M. Lau, "Bufferless III–V photodetectors directly grown on (001) silicon-on-insulators," Opt. Lett. **45**, 1754–1757 (2020).
225. B. Kunert, W. Guo, Y. Mols, R. Langer, and K. Barla, "Integration of III/V hetero-structures by selective area growth on Si for nano-and optoelectronics," ECS Trans. **75**, 409–419 (2016).
226. M. Baryshnikova, Y. Mols, Y. Ishii, R. Alcotte, H. Han, T. Hantschel, O. Richard, M. Pantouvaki, J. Van Campenhout, D. Van Thourhout, R. Langer, and B. Kunert, "Nano-ridge engineering of gasb for the integration of InAs/GaSb heterostructures on 300 mm (001) Si," Crystals **10**, 330 (2020).
227. Y. Shi, M. Pantouvaki, J. Van Campenhout, D. Colucci, M. Baryshnikova, B. Kunert, and D. Van Thourhout, "Loss-coupled DFB nano-ridge laser monolithically grown on a standard 300-mm Si wafer," Opt. Express **29**, 14649–14657 (2021).
228. D. Colucci, M. Baryshnikova, Y. Shi, Y. Mols, M. Muneeb, Y. De Koninck, D. Yudistira, M. Pantouvaki, J. Van Campenhout, R. Langer, D. Van Thourhout, and B. Kunert, "Unique design approach to realize an O-band laser monolithically

integrated on 300 mm Si substrate by nano-ridge engineering," Opt. Express **30**, 13510–13521 (2022).

229. Y. Shi, B. Kunert, Y. De Koninck, M. Pantouvaki, J. Van Campenhout, and D. Van Thourhout, "Novel adiabatic coupler for III–V nano-ridge laser grown on a Si photonics platform," Opt. Express **27**, 37781–37794 (2019).
230. Y. Mols, A. Vais, S. Yadav, L. Witters, K. Vondkar, R. Alcotte, M. Baryshnikova, G. Boccardi, N. Waldron, B. Parvais, N. Collaert, R. Langer, and B. Kunert, "Monolithic integration of nano-ridge engineered InGaP/GaAs HBTs on 300 mm Si substrate," Materials **14**, 5682 (2021).
231. C. I. Ozdemir, Y. De Koninck, D. Yudistira, N. Kuznetsova, M. Baryshnikova, D. Van Thourhout, B. Kunert, M. Pantouvaki, and J. Van Campenhout, "Low dark current and high responsivity 1020nm InGaAs/GaAs nano-ridge waveguide photodetector monolithically integrated on a 300-mm Si wafer," J. Lightwave Technol. **39**, 5263–5269 (2021).
232. M. Scherrer, N. V. Triviño, S. Mauthe, P. Tiwari, H. Schmid, and K. E. Moselund, "In-plane monolithic integration of scaled III–V photonic devices," Appl. Sci. **11**, 1887 (2021).
233. H. Schmid, M. Borg, K. Moselund, L. Gignac, C. M. Breslin, J. Bruley, D. Cutaia, and H. Riel, "Template-assisted selective epitaxy of III–V nanoscale devices for co-planar heterogeneous integration with Si," Appl. Phys. Lett. **106**, 233101 (2015).
234. S. Wirths, B. F. Mayer, H. Schmid, M. Sousa, J. Gooth, H. Riel, and K. E. Moselund, "Room-temperature lasing from monolithically integrated GaAs microdisks on silicon," ACS Nano **12**, 2169–2175 (2018).
235. B. F. Mayer, S. Wirths, S. Mauthe, P. Staudinger, M. Sousa, J. Winiger, H. Schmid, and K. E. Moselund, "Microcavity lasers on silicon by template-assisted selective epitaxy of microsubstrates," IEEE Photonics Technol. Lett. **31**, 1021–1024 (2019).
236. P. Tiwari, P. Wen, D. Caimi, S. Mauthe, N. V. Triviño, M. Sousa, and K. E. Moselund, "Scaling of metal-clad InP nanodisk lasers: optical performance and thermal effects," Opt. Express **29**, 3915–3927 (2021).
237. S. Mauthe, P. Tiwari, M. Scherrer, D. Caimi, M. Sousa, H. Schmid, K. E. Moselund, and N. V. Triviño, "Hybrid III–V silicon photonic crystal cavity emitting at telecom wavelengths," Nano Lett. **20**, 8768–8772 (2020).
238. S. Mauthe, Y. Baumgartner, M. Sousa, Q. Ding, M. D. Rossell, A. Schenk, L. Czornomaz, and K. E. Moselund, "High-speed III–V nanowire photodetector monolithically integrated on Si," Nat. Commun. **11**, 4565–4567 (2020).
239. J. Manigrasso, I. Chilln, V. Genna, P. Vidossich, S. Somarowthu, A. M. Pyle, M. De Vivo, and M. Marcia, "Waveguide coupled III–V photodiodes monolithically integrated on Si," Nat. Commun. **13**, 1–11 (2022).
240. V. Djara, V. Deshpande, E. Uccelli, N. Daix, D. Caimi, C. Rossel, M. Sousa, H. Siegwart, C. Marchiori, J.M. Hartmann, K.-T. Shiu, C.-W. Weng, M. Krishnan, M. Lofaro, R. Steiner, D. Sadana, D. Lubyshev, A. Liu, L. Czornomaz, and J. Fompeyrine, "An InGaAs on Si platform for CMOS with 200 mm InGaAs-OI substrate, gate-first, replacement gate planar and FinFETs down to 120 nm contact pitch," in *2015 Symposium on VLSI Technology (VLSI Technology)*, pp. T176–T177. IEEE, 2015.
241. O. Parillaud, E. Gil-Lafon, B. Gérard, P. Etienne, and D. Pribat, "High quality InP on Si by conformal growth," Appl. Phys. Lett. **68**, 2654–2656 (1996).
242. W. Metaferia, H. Kataria, Y.-T. Sun, and S. Lourdudoss, "Growth of InP directly on Si by corrugated epitaxial lateral overgrowth," J. Phys. D: Appl. Phys. **48**, 045102 (2015).

243. Z. Yan, Y. Han, L. Lin, Y. Xue, C. Ma, W. K. Ng, K. S. Wong, and K. M. Lau, "A monolithic InP/SOI platform for integrated photonics," Light: Sci. Appl. **10**, 200 (2021).
244. Y. Han, Y. Xue, and K. M. Lau, "Selective lateral epitaxy of dislocation-free InP on silicon-on-insulator," Appl. Phys. Lett. **114**, 192105 (2019).
245. Y. Han, Z. Yan, Y. Xue, and K. M. Lau, "Micrometer-scale InP selectively grown on SOI for fully integrated Si-photonics," Appl. Phys. Lett. **117**, 052102 (2020).
246. Y. Xue, Y. Han, Y. Tong, Z. Yan, Y. Wang, Z. Zhang, H. K. Tsang, and K. M. Lau, "High-performance III–V photodetectors on a monolithic InP/SOI platform," Optica **8**, 1204–1209 (2021).
247. T. Fujii, K. Takeda, H. Nishi, N.-P. Diamantopoulos, T. Sato, T. Kakitsuka, T. Tsuchizawa, and S. Matsuo, "Multiwavelength membrane laser array using selective area growth on directly bonded InP on SiO 2/Si," Optica **7**, 838–846 (2020).

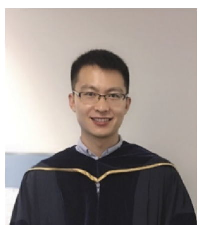

Yu Han received the B.S. degree from the Huazhong University of Science and Technology, Wuhan, in 2014, and the Ph.D. degree from the Hong Kong University of Science and Technology, Hong Kong, in 2018. He is currently an Associate Professor at School of Electronics and Information Technology, Sun Yat-sen University. His current research focuses on the monolithic integration of III–V optoelectronic devices on Si via selective heteroepitaxy.

Hyundai Park received the B.S. degree in electrical engineering from Seoul National University, Korea in 2000, and the Ph.D. degree in electrical and computer engineering from the University of California Santa Barbara (UCSB) in 2008. Since 2008, he has held various positions in the photonics industry to commercialize silicon photonic integrated circuits for data communication and sensing applications at Intel, Aurrion/Juniper, and Nexus Photonics.

John Bowers holds the Fred Kavli Chair and is the Director of the Institute for Energy Efficiency and a Distinguished Professor in the ECE and Materials Departments at UCSB. He is a member of the National Academy of Engineering and is an AAAS, Optica, IEEE, and APS fellow. He is a recipient of the IEEE Photonics, Optica/IEEE Tyndall, Optica Holonyak, and IEEE William Streifer Awards.

Kei May Lau is Chair Professor of ECE at HKUST. She received her B.S. and M.S. degrees in physics from the University of Minnesota, Minneapolis, and Ph.D. degree in Electrical Engineering from Rice University in Houston, Texas. After a two-year stint in the industry, she joined the faculty of the ECE Department at the University of Massachusetts/Amherst. She has been on the faculty of HKUST since 2000 and established the Photonics Technology Center for research in compound semiconductor materials and devices. She is a Fellow of the IEEE, Optica, and the Hong Kong Academy of Engineering Sciences. She is also a recipient of the IET J. J. Thomson medal for Electronics, the Optica (OSA) Nick Holonyak Jr. Award, the IEEE Photonics Society Aron Kressel Award, the US National Science Foundation (NSF) Faculty Awards for Women (FAW)

Scientists and Engineers, and a Hong Kong Croucher Senior Research Fellowship. She was an Editor of the *IEEE Transactions on Electron Devices* and *Electron Device Letters* and an Associate Editor for the *Journal of Crystal Growth* and *Applied Physics Letters*. Her research work is focused on the development of monolithic integration of semiconductor devices on industry-standard silicon substrates.

143.89.78.41 {ts '2023-01-09 00:28:57'}